JOURNAL OF GEOPHYSICAL RESEARCH, VOL. 111, A12103, doi:10.1029/2006JA011871, 2006

Coronal prominence structure and dynamics: A magnetic flux rope interpretation

S. E. Gibson[1] and Y. Fan[1]

Received 25 May 2006; revised 17 August 2006; accepted 15 September 2006; published 9 December 2006.

[1] The solar prominence is an example of a space physics phenomenon that can be modeled as a twisted magnetic flux tube or magnetic flux "rope." In such models the prominence is one observable part of a larger magnetic structure capable of storing magnetic energy to drive eruptions. We show how a flux rope model explains a range of observations of prominences and associated structures such as cavities and soft X-ray sigmoids and discuss in particular the observational and dynamic consequences of three-dimensional reconnections in and around the evolving magnetic flux rope. We demonstrate that the flux rope model can describe the prominence's preeruption structure and dynamics, loss of equilibrium, and behavior during and after an eruption in which part of the flux rope is expelled from the corona.

Citation: Gibson, S. E., and Y. Fan (2006), Coronal prominence structure and dynamics: A magnetic flux rope interpretation, *J. Geophys. Res.*, *111*, A12103, doi:10.1029/2006JA011871.

1. Introduction

[2] Coronal mass ejections (CMEs) are arguably the most important solar drivers of space weather [*Lindsay et al.*, 1999; *Webb et al.*, 2000]. A CME corresponds to a spontaneous eruption of closed magnetic fields previously in equilibrium. It results in an explosive release of the free magnetic energy stored in the preeruption helical (i.e., twisted or sheared) magnetic fields [see review by *Priest and Forbes*, 2002]. The storage and release of magnetic energy in a CME thus critically depends upon the form of these preeruption magnetic fields.

[3] As soon as CMEs were regularly observed, it became apparent that they were often associated with prominence eruptions [*Gosling et al.*, 1974]. Prominences are long-lived coronal structures that are two orders of magnitude more cool and dense than the surrounding coronal atmosphere in which they are suspended. When they are viewed at the solar limb they are referred to as "prominences" (Figures 1a–1c)), and when they are viewed against the solar disk (e.g., Figure 2b), they are referred to as "filaments." We will use both terms interchangeably in this paper. Erupting prominences can be identified as bright cores of CMEs when observed by white light coronagraphs [*Illing and Hundhausen*, 1986]. Thus it is clear that understanding the magnetic structure of the prominence and any associated coronal phenomena is key to understanding both the CME and the pre-CME magnetic equilibrium state.

[4] We have previously used three-dimensional (3-D) magnetohydrodynamic (MHD) numerical simulations to model CMEs in terms of magnetic flux ropes emerging into the corona. As the rope emerges, the coronal field quasi-statically evolves through increasingly energized equilibria, until a magnetic twist threshold is crossed, leading to loss of equilibrium and eruption [*Fan*, 2005; *Gibson and Fan*, 2006]. In this paper we examine the observable properties of prominences and associated coronal structures as predicted by our simulations, before, during, and after eruption. Our simulations also provide us with a rich resource for exploring the role of three-dimensional reconnections in the evolution of the prominence, so we consider a variety of such reconnections in detail. In section 2 we review the long history of modeling the prominence as a flux rope and discuss how observed coronal features commonly associated with prominences, i.e., prominence cavities and soft X-ray sigmoids, can also be described by flux rope models. In section 3 we describe our numerical model, and in section 4 we present the observables predicted by a simulation of an equilibrium flux rope representative of the preeruption, energy storage stage. In section 5 we consider the observables predicted by a simulation of a flux rope which loses equilibrium and erupts, breaking in two in the process. We also present an in-depth analysis of three-dimensional reconnections in this section. In section 6 we discuss the conditions under which a flux rope might break in two during eruption. In section 7 we present our conclusions.

2. Background

2.1. A Model for Prominences: Magnetic Flux Rope

[5] A twisted magnetic flux rope is an appealing model for the prominence because its helical field lines provide support for the mass of the prominence and are capable of storing the free magnetic energy needed to drive a CME. Here we define a coronal flux rope as a magnetic structure that contains field lines that twist about each other by more than one wind between the two ends anchored to the

[1]High Altitude Observatory, National Center for Atmospheric Research, Boulder, Colorado, USA.

0148-0227/06/2006JA011871$09.00

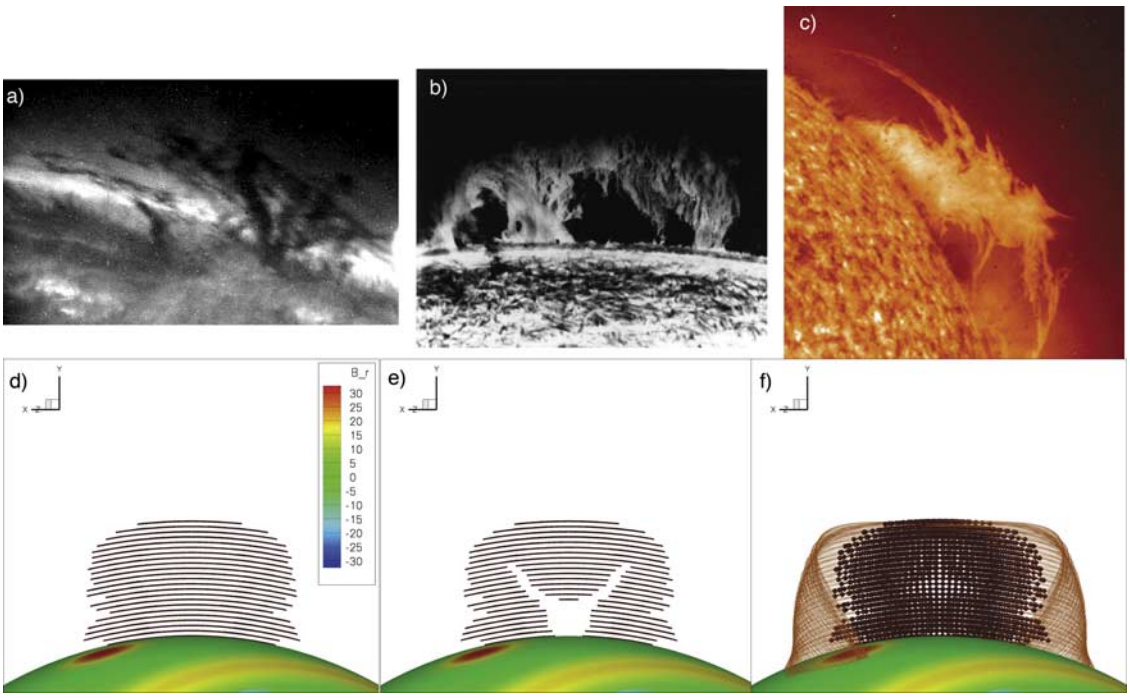

Figure 1. Observations of quiescent (noneruptive) solar prominences: (a) TRACE Fe IX/X 171 Å (in absorption), (b) BBSO H-α, and (c) SOHO/EIT He II 304 Å. Model prominences corresponding to *Fan and Gibson* [2006] prediction of magnetic flux rope in equilibrium: (d) field line dips filled to prominence scale height (0.001 $R_\odot$ from dip base) (e) dips plotted only if on field lines not intersecting current sheet as shown in Figures 2 and 4, and (f) dips as in Figure 1d along with light brown field line extensions representing dynamic portion of prominence associated with shallow dips (see text). The normal magnetic field is shown in Figures 1d–1f with contour levels identified in units of Gauss. Movies showing rotating in three dimensions as in Figures 1d–1f can be found in the electronic version of this paper.

photosphere [*Low*, 2001]. A wide variety of magnetic structures which can be classified as flux ropes have been employed in modeling prominences. Three-dimensional idealized models range from slightly twisted ropes that wind less than twice around their axis [*Gibson et al.*, 2004], to slinky-type ropes that are more tightly wound [*Amari et al.*, 1999], to more complex structures based on a spheromak topology [*Lites and Low*, 1997; *Gibson and Low*, 1998, 2000]. More observationally based models have also been employed [*Aulanier and Demoulin*, 1998; *van Ballegooijen*, 2004]. Flux rope models have been shown to explain a range of observed prominence properties, including prominence formation, structure and evolution, and ultimately eruption.

2.1.1. Prominence (Flux Rope) Formation

[6] Even in the context of the flux rope model, flux rope formation and prominence formation are not necessarily equivalent. Rather, the formation of a coronal equilibrium flux rope is a necessary but not sufficient condition for prominence formation in such models. We will discuss this in more detail in the next section.

[7] Our first consideration is to address how magnetic flux rope equilibria might form in the corona. One possibility is that ropes emerge from below the solar photosphere, having been already formed in the solar interior [*Rust and Kumar*, 1994; *Low*, 1996; *Fan*, 2001; *Magara and Longcope*, 2001; *Abbett and Fisher*, 2003; *Archontis et al.*, 2004; *Amari et al.*, 2004a, 2004b]. Such a hypothesis is borne out by theoretical studies, implying the structural necessity of twist in magnetic flux tubes rising through the solar convection zone [*Emonet and Moreno-Insertis*, 1998; *Fan et al.*, 1998; *Abbett et al.*, 2000] and by observations indicating the emergence of pretwisted magnetic fields through the solar photosphere [*Tanaka*, 1991; *Leka et al.*, 1996]. On the other hand, models of the dynamic transport of flux ropes from the interior into the corona have indicated that it is not easy for dipped magnetic field to cross the dense photosphere [*Fan*, 2001; *Magara*, 2004]. A recent analysis of a shorter, less twisted flux rope has demonstrated that it is possible for a rope to partly emerge, by virtue of self-induced shear due to the Lorentz force and subsequent internal reconnections as the rope expands up into the corona [*Manchester et al.*, 2004]. This and other simulations [*Longcope and Welsch*, 2000; *Amari et al.*, 2004b; *Archontis et al.*, 2005] indicate that even when a flux rope does not smoothly emerge across the photosphere, most or all of its axial flux can still be transported into the corona. We will return to this issue below in section 3.

[8] Shearing motions at the photosphere have also been invoked to create coronal magnetic flux ropes. Simulations in which an initially untwisted coronal flux tube is sheared at its footpoints have led to a loosely wound (less than two full turns) flux rope in equilibrium [*Toeroek and Kliem*, 2003] or, alternatively, to more tightly wound flux ropes formed by reconnections which are immediately unstable and erupt [*Tokman and Bellan*, 2002; *Amari et al.*, 2003b].

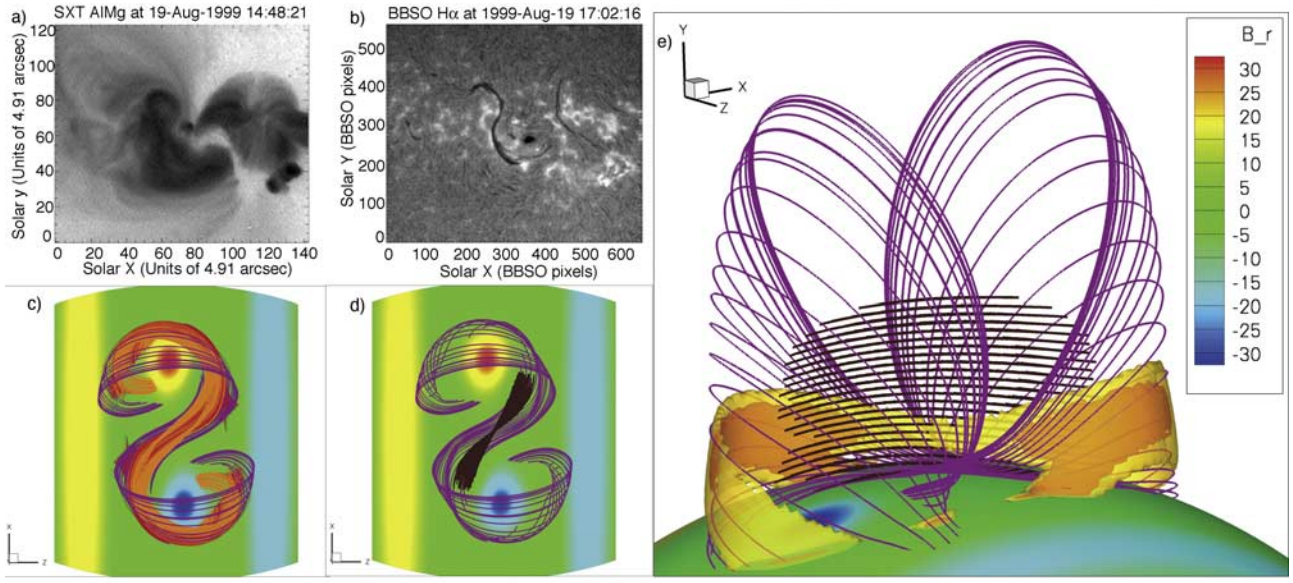

Figure 2. Observation of a quiescent sigmoid in (a) soft-X-ray (Yohkoh SXT) and (b) associated H-α filament (a.k.a. prominence) (BBSO) (from *Gibson et al.* [2002]). (c–e) Equilibrium magnetic flux rope model as in Figure 1. Magenta field lines are representative of the bald-patch-separatrix surface (BPSS) that separates winding and non-winding field lines, and brown indicates dips in magnetic field lines at all heights as in Figure 1d. Yellow and orange isosurfaces in Figure 2e show current sheet as defined in text. Red and orange field lines shown in Figure 2c intersect the orange isosurface of current sheet shown in Figure 2e: orange lines are the subset that are dipped (the dips associated with these current-sheet intersecting orange field lines are the ones excluded from the filament representation of Figure 1e). The normal magnetic field is shown in Figures 2c–2e with contour levels identified in units of Gauss. A movie showing rotating in three-dimensions as in Figure 2e can be found in the electronic version of this paper.

In the simulations of *Kusano et al.* [2004] and *Kusano* [2005], a rope is formed as shearing motions lead to reconnections driven by the resistive tearing mode instability. Another possibility is flux rope formation as a result of a more gradual diffusion of decaying active region flux on the photosphere [*van Ballegooijen et al.*, 1998, 2000; *Mackay and van Ballegooijen*, 2001, 2005, 2006; *Amari et al.*, 2003a]. In particular the large-scale quiescent prominences associated with decaying active regions are most likely formed in this fashion. Finally, a coronal flux rope can be created by the process known as "flux cancellation," which may be interpreted as either mimicking the emergence of a subphotospheric flux rope, or as arising from a combination of photospheric shearing flows and the emergence or submergence of opposite polarities (which is equivalent to flux cancellation) [*van Ballegooijen and Martens*, 1999; *Amari et al.*, 2000; *Linker et al.*, 2003]. Such a technique can lead to a flux rope in equilibrium or, if flux cancellation is continued, to an eruption (see below).

[9] In most of the above scenarios of flux rope formation, magnetic reconnection plays a fundamental role in liberating excess magnetic energy. It is important to note that in spite of such reconnections, the magnetic field does not generally relax to a potential state. This is because reconnection under high electrical conductivity approximately conserves the global magnetic helicity [*Berger and Field*, 1984]. Thus coronal fields will naturally produce a flux rope, rather than a potential field, as a metastable state (see, e.g., review by *Zhang and Low* [2005]).

2.1.2. Prominence Structure and Evolution

[10] It has long been noted [*Kuperus and Raadu*, 1974; *Priest et al.*, 1989; *Rust and Kumar*, 1994] that once an equilibrium flux rope is formed in the corona, by whatever means, the dips in the helical field lines naturally provide support for the dense, cool prominence/filament material against gravity. Flux rope models also explain the magnetic inverse configuration (where the field across the filament is opposite to that predicted by a potential field anchored to the photosphere below) that is observed in many prominences [*Leroy et al.*, 1984]. Observed filament properties such as the orientation of filament threads relative to underlying magnetic field (e.g., filament chirality), and "barbs" protruding from the side of the filament [*Martin*, 1998] have been explained in terms of idealized flux rope models [*Rust and Kumar*, 1994; *Low and Hundhausen*, 1995; *Gibson and Low*, 2000] and are well-matched by observationally constrained flux rope models [*Aulanier and Demoulin*, 1998; *van Ballegooijen*, 2004].

[11] As mentioned above, the existence of dipped magnetic field lines does not necessarily mean that these dips will be filled with prominence mass. The filament "channel," a region of depleted coronal density in which a filament may or may not be centered, is more frequently observed than the filament itself, possibly indicating that a magnetic environment capable of supporting a filament

exists even if the filament does not (see also discussion below on cavities). Several mechanisms have been proposed for the origins of prominence mass. One possibility is that coronal plasma condenses to form the prominence, in the process also draining the surrounding corona and accounting for the sparse filament channel or cavity [*Pneuman*, 1983]. However, observations indicate that more mass is required to form the prominence than exists in nearby coronal material [*Saito and Tandberg-Hanssen*, 1973], so such condensing mass would have to originate from below, for example as might be transported upward by spicules [*Athay and Holzer*, 1982; *An et al.*, 1985]. Another possibility is that chromospheric mass is scooped up by the dipped fields of emerging flux ropes [*Rust and Kumar*, 1994] or by reconnections at the photosphere [*Galsgaard and Longbottom*, 1999; *Litvinenko and Wheatland*, 2005]. Still another possibility is that localized chromospheric heating causes siphon flow of material along field lines that condenses and forms the prominence [*Antiochos et al.*, 1999b]. Whatever mechanism is invoked, whether or not a filament channel is filled is likely to depend on the combined magnetic, thermal, and dynamic details of the local environment, as well as the history of the region.

[12] Observations demonstrate that prominence mass is often very dynamic, with counterstreaming flows observed along the central filament spine and in its barbs [*Zirker et al.*, 1998; *Martin*, 1998], and apparently helical motions in active (but noneruptive) prominences [*Gilbert et al.*, 2001]. Such prominence motions have been explained in terms of reconnection [*Gilbert et al.*, 2001; *Petrie and Low*, 2005; *Litvinenko and Wheatland*, 2005], steady rigid motions of adjacent prominence sheets in local force equilibria [*Low and Petrie*, 2005], and thermal nonequilibrium of prominence plasma [*Antiochos et al.*, 2000; *Karpen et al.*, 2003, 2005, 2006]. The latter analyses were performed on sheared, dipped arcade fields rather than flux ropes (it has even been proposed that dips are not necessary for filament support: in sufficiently flat-topped arcade fields, a steady-state dynamic solution can be found to represent the filament [*Karpen et al.*, 2001]). In such thermal nonequilibrium models, and also in a thermal-hydrodynamic model which was applied to a magnetic flux rope geometry [*Lionello et al.*, 2002], it was found that whether or not prominence mass condensed and was dynamic depended sensitively on choices of model parameters and heating functions. In general terms, it is likely that nonsteady prominence mass motions are a natural consequence of the time-varying local thermodynamic and magnetic environment in which they are embedded.

2.1.3. Prominence Eruption

[13] Observations of coronal mass ejections and erupting prominences are commonly interpreted as magnetic flux ropes [*Dere et al.*, 1998; *Plunkett et al.*, 2000; *Cremades and Bothmer*, 2004]. The origins of these erupting ropes are controversial, however; in some models the flux rope forms during the eruption [*Gosling et al.*, 1995; *Tokman and Bellan*, 2002; *Amari et al.*, 2003b; *Lynch et al.*, 2004; *Manchester et al.*, 2004; *Kusano et al.*, 2004]. In other models, the magnetic flux rope exists prior to the eruption as an magnetohydrodynamic (MHD) equilibrium state. Such a twisted magnetic flux rope equilibrium may exist stably for long periods of time in the corona, supporting a quiescent prominence and storing the magnetic energy that ultimately will drive its eruption. Eventually, the addition of even a small amount of twisted magnetic flux with respect to the confining overlying field could trigger an explosive release of the stored free magnetic energy in a CME [*Sturrock et al.*, 2001; *Priest and Forbes*, 2002]. Catastrophic loss of equilibrium of 2-D flux rope configurations has been shown analytically [*Forbes and Priest*, 1995; *Lin et al.*, 1998]. Loss of equilibrium and eruptive behavior of both 2-D and 3-D twisted flux rope configurations have also been shown in numerical simulations [*Linker et al.*, 2001; *Amari et al.*, 2000, 2003a, 2004a, 2004b; *Toeroek and Kliem*, 2003; *Kusano et al.*, 2004; *Roussev et al.*, 2004; *Kusano*, 2005; *Fan*, 2005; *Toeroek and Kliem*, 2005; *Fan and Gibson*, 2006; *Gibson and Fan*, 2006; *Mackay and van Ballegooijen*, 2006]. We will discuss this in more detail in section 5.

2.2. Observables Associated With Prominences

2.2.1. Prominence Cavities

[14] White light coronagraph observations often show a cavity, which may surround a prominence, both in a quiescent state prior to an eruption (Figure 3a) and as an aspect of CMEs (Figures 8a–8d) [*Gibson et al.*, 2006b, and references therein]. Magnetic flux rope models explain the filament and cavity as two parts of the same magnetic structure. The sharply defined cavity arises from strong internal magnetic pressure and winding field lines that are partially detached from the photosphere [*Low*, 1996], and the prominence, as discussed above, is supported in the dips of the magnetic field. The cavity is the upper coronal part of a filament channel and, like the filament channel, can exist with or without an associated filament. Indeed, *Gibson et al.* [2006b] found that cavities as observed in the low corona in white light are ubiquitous, with several cavities often apparent on any given day. Just as filaments vary in size and location, from lower-latitude, active region-associated filaments, to high-latitude, polar crown filaments, so do their associated cavities. Cavity visibility in white light depends on the projection of density along the line of sight; thus the large, longitudinally extended polar crown filament-related cavities are the most easily detectable, visible for days and even weeks at a time. A cavity can erupt with its entrained filament as a CME, and the fact that such an eruption appears to be a bodily lifting-off of the pre-CME filament and cavity argues strongly for the loss of equilibrium of a preexisting magnetic flux rope structure, as shown in Figure 8e–8h and discussed below in section 5.4. Even after eruption, a remnant of the cavity and filament often remains or reforms, and polar crown filament-related cavities in particular can be identified as large-scale coronal magnetic structures that exist for months.

2.2.2. Sigmoids and Other Soft X-Ray Features

[15] Another set of structures linked to CMEs are soft X-ray sigmoids, or hot, S-shaped regions [*Rust and Kumar*, 1996; *Sterling and Hudson*, 1997; *Canfield et al.*, 1999] (Figure 2a). They exist not just during eruption, but quiescently, and are often associated with a filament, which sometimes itself possesses a sigmoidal shape (Figure 2b) [*Manoharan et al.*, 1996; *Rust and Kumar*, 1994; *Pevtsov*, 2002a, 2002b; *Lites and Low*, 1997; *Gibson et al.*, 2002]. Magnetic flux ropes and associated S-shaped field lines

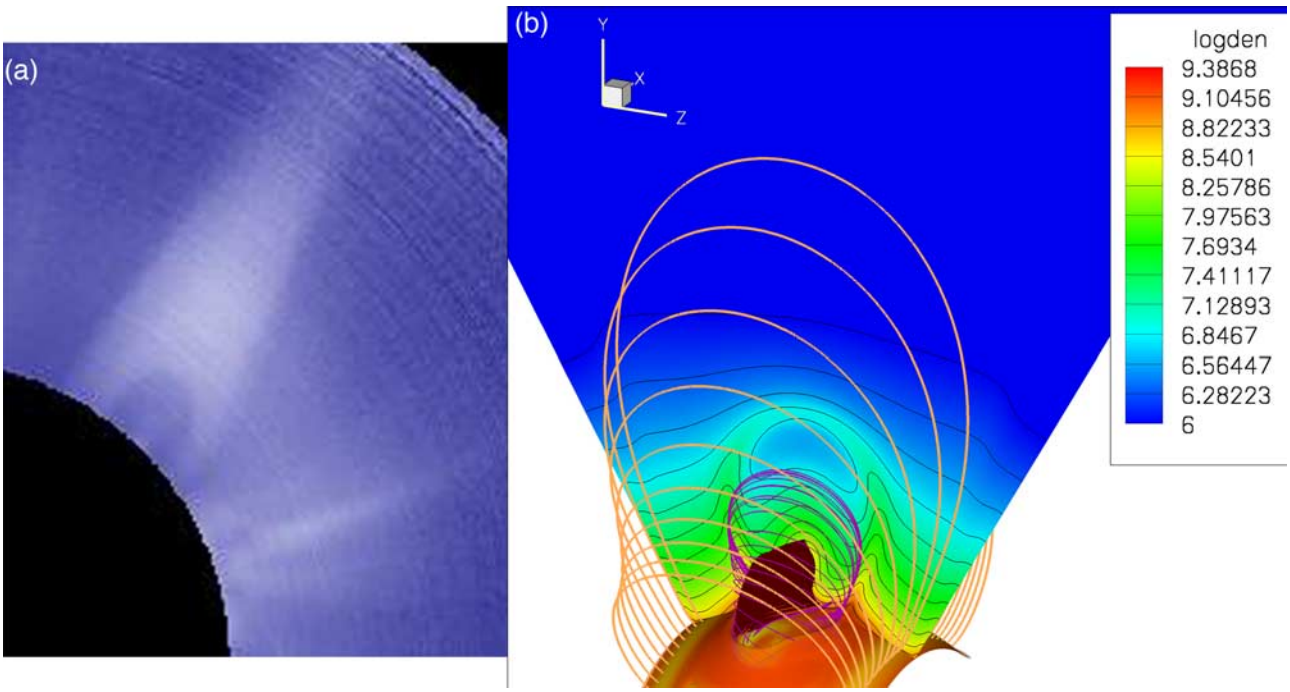

Figure 3. (left) Observation of pre-CME prominence with cavity (HAO/MLSO, white light, 22 July 2002). (right) *Fan and Gibson* [2006] three-dimensional (3-D) flux rope equilibrium. Isosurface and isocontours show the logarithm of density, dipped field capable of holding prominence mass is shown in brown, magenta lines show the bald-patch-separatrix-surface (BPSS) of dipped field just grazing the "photosphere" (e.g., the simulation's lower boundary), and yellow lines show overlying arcade field. Isosurface and isocontours show the logarithm of number density (in cgs units).

have often been proposed as models for soft X-ray sigmoids [*Rust and Kumar*, 1996; *Amari et al.*, 2000, 2003b; *Magara and Longcope*, 2001; *Kliem et al.*, 2004; *Kusano*, 2005; *Aulanier et al.*, 2005].

[16] It is important, however, to consider why sigmoidal field lines of a particular direction (i.e., forward versus backward-S shaped) would be heated in such flux rope models (see detailed discussion in the work of *Gibson et al.* [2006a]). One possibility is that the field lines being heated represent a topological surface where tangential discontinuities are likely to arise, leading to current sheet formation and reconnections [*Parker*, 1994; *Titov and Demoulin*, 1999; *Low and Berger*, 2003]. The magenta lines in the flux rope images of Figures 2c–2e represent such a topological surface. The bald patch (BP) of a coronal magnetic field structure is defined as the locus of points where dipped field just touches the photosphere (i.e., at the centers of the magenta field lines) [*Titov et al.*, 1993]. The bald-patch-separatrix surface (BPSS, magenta field lines) is made up of the field lines that contain the BP points. Current sheets tend to form along the BPSS because it represents a discontinuous transition in the dynamic behavior between the helical field lines that are locally detached from the photosphere and the neighboring anchored field lines. Reconnections at this current sheet would then yield the heating that creates the emission of the soft X-ray sigmoid.

[17] Since the BPSS represents a "fault line" in the coronal magnetic field across which field lines behave very differently when driven dynamically, not only a rope eruption but any dynamic perturbation such as flux emergence or photospheric motions could cause the development of magnetic tangential discontinuities (or current sheets) along the BPSS. We will demonstrate this explicitly for a flux rope filament model with a sigmoidal BPSS in sections 4 and 5 below. In the case of a longitudinally extended filament (such as a polar crown filament) which may be represented by a quasi-2D flux rope (with symmetry about the axis of solar rotation), the BPSS takes the form of a tunnel or sheath around the photosphere-grazing portion of the flux rope. Idealized simulations of a 2-D axisymmetric toroidal flux rope show current sheets forming along the BPSS within the confined flux rope during its quasistatic evolution [*Fan and Gibson*, 2006]. The heating resulting from the dissipation of this current sheet combined with the million degree thermal conduction of the corona may produce a hot sheath surrounding the prominence, providing a plausible explanation for the soft X-ray bright sources within cavities of stable polar crown filament channels [*Hudson et al.*, 1999].

3. Modeling Equilibria and Eruption of Magnetic Flux Ropes

[18] We simulate the evolutionary transport of a twisted magnetic structure (i.e., an arched flux rope) through a lower boundary (which we will identify with the solar photosphere) into a preexisting, initially potential coronal field. We employ a three-dimensional model in spherical geometry, by numerically solving the MHD equations under isothermal conditions. The emerging flux rope is not ini-

tially force free; it is transported into the computational domain (corona) via the time-dependent electric field at the lower boundary and then allowed to relax dynamically in that domain to a nearly force-free configuration. Thus, although the numerical simulation effectively transports the flux rope as a rigid structure across the "photosphere," once in the corona it can evolve and modify its initial form, as governed by the isothermal MHD equations. The rope emergence is driven at a constant speed, until we stop the rise and anchor the field lines by setting the electric field at the lower boundary to zero. We refer the reader to *Fan* [2005] for further details on the model.

[19] The imposed kinematic flux emergence at the lower boundary is a means to construct a sequence of 3-D near-force-free coronal flux rope equilibria with increasing amounts of detached, twisted flux so as to investigate their stability and eruptive dynamics. As discussed above, the flux rope may form in the corona via a variety of mechanisms, and not necessarily be due to direct emergence from the interior. However, for many of those mechanisms (e.g., rotational footpoint motion, flux cancellation, turbulent diffusion...) the net effect is a gradual build-up of a flux rope containing helical field lines with strong axial field above the polarity inversion line. We submit that such general flux rope equilibria are well described by our simulations, even though we should keep in mind that they may actually be formed in different ways.

[20] As the flux rope in our simulation emerges into the corona, we find two distinct stages of the evolution of the coronal magnetic field. The initial evolution is quasi-static during which the magnetic energy transported into the corona is being stored in a sequence of confined flux rope equilibria. This is followed by a dynamic stage in which the flux rope loses confinement and erupts. If emergence is stopped before the dynamic stage is reached, a noneruptive, force-free equilibrium is found. In the next two sections, we will first use such a noneruptive, equilibrium flux rope simulation [*Fan and Gibson*, 2006] to consider the observable pre-CME properties of the filament and related structures and then use a simulation where emergence was continued to the point of loss of equilibrium [*Gibson and Fan*, 2006] to consider their observable and reconnection properties during eruption.

4. Energy Storage Stage: Pre-CME Flux Rope

4.1. A Model for the Quiescent Prominence

[21] Figures 1–3 show the three-dimensional, magneto-hydrodynamic equilibrium flux rope configuration described by *Fan and Gibson* [2006]. The dipped portion of the field, where filament mass may be supported, is shown in dark brown. Figures 1, 2e, and 3b represent views from the side, analogous to solar limb viewing angles for prominences. From these (and from the online edition movies) it is clear that this collection of field line dips forms a thin, curved sheet suspended above the photospheric neutral line (which separates positive and negative normal magnetic field).[1] Figure 2d shows a top-down view, analogous to viewing a filament at disk center, and shows that our modeled structure is comparable to observed, sigmoid-shaped filaments such as shown in Figure 2b.

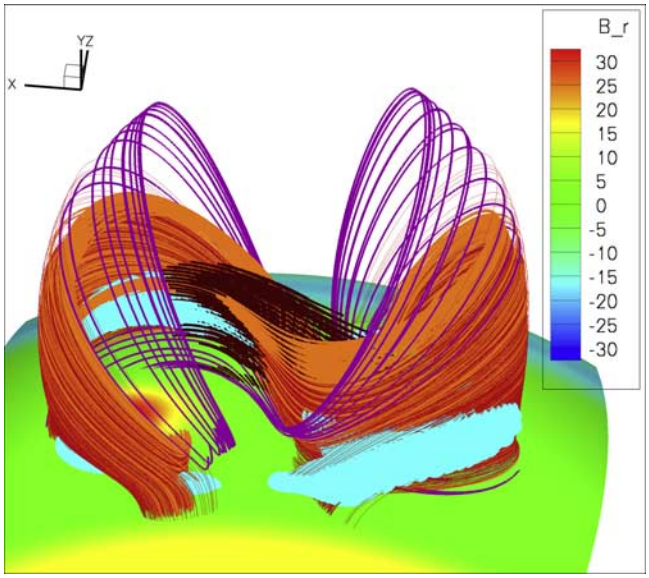

Figure 4. Equilibrium flux rope representation of filament dips, current sheets, and associated sigmoidal field lines. Magenta field lines show BPSS. Brown indicates dips in magnetic field lines at all heights as in Figure 1d. The dark orange isosurface in Figure 2e is shown here in turquoise, and indicates a current sheet as defined in the text. Red and orange field lines intersect this turquoise current sheet surface: orange lines are the subset that are dipped (the dips associated with these current-sheet-intersecting orange field lines are the ones excluded from the filament representation of Figure 1e). The normal magnetic field is shown with contour levels identified in units of Gauss. A movie showing this structure rotating in three dimensions can be found in the electronic version of this paper.

[22] In Figures 1d, 2d, 2e, and 3b, the prominence is represented as dips in magnetic field lines, and we have followed the scheme used by *Aulanier and Demoulin* [1998] in filling the dips up to approximately a prominence pressure scale height. However, as we have discussed above, local thermodynamic conditions are likely to determine which, if any, of these dips will actually be filled, and whether the mass in them will be static or dynamic. To self-consistently model the cool, dense filament mass in our three-dimensional magnetic structure, we should properly treat the thermodynamics along a set of representative field lines in a manner akin to that of *Lionello et al.* [2002] and [*Karpen et al.*, 2006]. We leave this for a future project. For now, we content ourselves with considering what the magnetic structure may tell us about where the prominence is likely to form and how this compares to observations.

[23] When we fill all the dips as in Figure 1d our prominence sheet is monolithic, and extends down to the "photosphere" (e.g., the simulation's lower boundary). This matches some observed prominences fairly well, e.g., Figure 1a. However, we note that this and many other prominences appear patchy, as they might if some of the dips were not filled. As we will discuss in more detail in

[1] Auxiliary materials are available in the HTML. doi:10.1029/2006JA011871.

section 4.2, we find that a current sheet (shown as yellow and orange isosurfaces in Figure 2) forms in close proximity to our filament dips. Indeed, some of the field lines possessing dips graze this current sheet, and, as we discuss below and demonstrate in Figure 4, may undergo reconnections. Filament material lying along such reconnecting field lines are likely to be heated to coronal temperatures, or to become dynamic, or both. We therefore show in Figure 1e a modeled prominence in which the dips from such current sheet-intersecting field lines have not been plotted. Note that this is more patchy than Figure 1d, and also that it possesses an arched shape reminiscent of those seen in prominences such as Figure 1b.

[24] We note that another way to model arched prominence structures as shown in Figure 1b is using flux ropes that possess a somewhat different topology than employed in our simulations, in that they have a magnetic X-line below the rope center. One way to visualize this is to imagine an emerging flux rope: once the axial field line has emerged, dipped magnetic field will intersect the photosphere at the center of the rope, forming a ''bald patch'' (BP) as discussed above. If the emergence continues, the central, dipped portion of the rope will lift up high enough so that it no longer intersects the photosphere, and the BP will bifurcate. A prominence modeled by filling the rope dips would then appear arch-like, with two ''legs'' extending down to the two BPs [*Aulanier and Demoulin*, 1998; *Titov and Demoulin*, 1999; *Gibson et al.*, 2003]. The central portion of such a rope will be topologically separated from the simple arcade field below it by a magnetic X-line along which the poloidal field comes to an X-point (the axial component of the field is not necessarily zero). We will discuss the significance of the presence or absence of such an X-line for eruption in more detail in section 6.

[25] Finally, we consider what the magnetic structure implies for dynamic versus static filament material. As discussed above, observations demonstrate that filament mass is often in motion, even in noneruptive (quiescent) prominences. *Antiochos et al.* [1999b] showed that in a long, sheared, dipped field line, heated near its chromospheric footpoints, thermal nonequilibrium led to the formation of condensations in the field line dip. In this analysis, the heating was applied symmetrically about the loop midpoint, and consequently, mass condensed in the dipped middle of the loop. In a subsequent analysis, *Antiochos et al.* [2000] found that when a greater amount of heating was applied to the left-hand loop footpoint than the right, the mass condensed at a point between the loop midpoint and the right footpoint. Moreover, rather than falling back down into the dipped middle of the loop, the mass moved uphill and over the rightmost looptop, ultimately following back down to the chromosphere on the right. Later analysis by *Karpen et al.* [2003] argued that whether or not the mass fell back down to pool at the middle dip, or rather moved up, over, and down to the chromosphere depended in part on the slope of the field line. Basically, if the component of gravitational force along the field line were sufficiently strong, as would be the case for a deeply dipped line, it would overcome the thermal pressure pushing it toward the nearby looptop and fall back into the dip. The authors quantified this slope in terms of the ratio between the dip depth as measured from a looptop to the loop half-length between the dip and that looptop and predicted the critical slope to be less than approximately 25% based on simple scaling arguments. They found that their simulations actually implied a critical slope of approximately half this value, which they suggested was due to the fact that mass continued to accrete after its initial condensation in their simulations, something not taken into account in the initial estimate of the critical slope.

[26] The critical slope estimate of *Karpen et al.* [2003] depended on a range of assumptions, including the degree of heating asymmetry and assumed radiative loss function, and a later analysis [*Karpen et al.*, 2005] also described how flux tube geometry was an additional factor in determining whether or not mass would be stationary or dynamic. The critical slope approach is nevertheless interesting, as it may be a means to determine if a given magnetic geometry could possibly yield dynamic filaments (via the thermal nonequilibrium method, anyway) under the right thermodynamic conditions. We therefore have determined which of our field lines possess a dip to length ratio (modified by $1/r^2$ for spherical coordinates) likely to yield dynamic versus static prominence material. We choose a very conservative critical slope of 5%, significantly less than that proposed by *Karpen et al.* [2003], in order to demonstrate that all of our dips are actually quite shallow. The light brown lines in Figure 1f indicate field line segments shown in entirety (from dip midpoint to field line endpoint) if they have upward slope less than 5%. The dips themselves, drawn only up to the prominence scale height, are shown in dark brown, as in Figure 1d–1e. Not all of the dip-containing field lines meet the critical slope criterion; indeed, most of the dipped field lines have one half that extends higher into the atmosphere, and possesses a steep slope (see, e.g., the magenta BPSS field lines of Figure 2e). However, the other halves of the dipped field lines lie lower and have much smaller slopes, and the light brown lines shown in Figure 1f are, in general, these flatter halves. Because of the symmetry of our rope, for every dipped field line with a shallow end to the right, there is an equivalent dipped line having its shallow end to the left. For this reason, essentially all filament mass condensing in our flux rope's dips has the potential to be dynamic. When triggered by localized heating at the footpoint opposite a field line's shallow half, filament mass could move up, over, and down that shallow half to the chromosphere, tracing out a light brown line segment and possibly explaining the arching ''spider'' type prominences as shown in Figure 1c, or even (when viewed end-on) spiral motions as discussed by *Gilbert et al.* [2001].

4.2. Current Sheet Formation and Reconnecting Field Lines

[27] As discussed above, the topological surface between winding and nonwinding fields, i.e., the BPSS, is expected to be a location for current sheet formation. We have previously demonstrated that current sheets do in fact form along this sigmoid-shaped surface in our simulations, both during eruption [*Fan and Gibson*, 2004; *Gibson et al.*, 2004; *Fan*, 2005], and in the quiescent, noneruptive flux rope equilibrium being discussed in this paper [*Fan and Gibson*, 2006]. The latter result is most relevant for observations of persistent, or noneruptive soft X-ray sigmoids.

[28] Figure 2e shows this current sheet (orange and yellow isosurfaces), along with the BPSS (magenta field lines). Such current sheets are significant to soft X-ray emission, as they are regions where field lines may be reconnecting and transferring magnetic energy to thermal energy, heating the field lines through thermal conduction in the process. These reconnected field lines, rather than the current sheet itself, are arguably the most appropriate proxies for the soft X-ray sigmoid [*Kliem et al.*, 2004].

[29] In our numerical calculations, the upwind, monotonicity preserving schemes used [*Stone and Norman*, 1992] provide an effective numerical diffusivity for the magnetic field that is dependent on the local gradient. In smoothly varying regions, the numerical diffusion is negligible. However, in regions of sharp gradients, where the magnetic field changes significantly over just a couple of grid cells, significant numerical diffusion (with an effective local diffusion coefficient η on the order of $\Delta x v_a$, where Δx is the grid cell size and v_a is the local Alfven speed) is automatically switched on. Thus significant magnetic reconnection due to the numerical diffusion is expected in these regions of sharp variations, which may correspond to physical current sheets.

[30] To identify these regions of significant magnetic reconnection, the current sheet isosurfaces plotted in this paper correspond to $J/B = |\nabla \times \mathbf{B}|/B \sim 1/l$, where l corresponds to the length scale of variation of $\mathbf{B}$ (a large value of $|\nabla \times \mathbf{B}|/B$ corresponds to a short length scale of variation). This is in contrast to our previous publications, in which we plotted isosurfaces of current density J. We find that the current sheets represented by isosurfaces of J/B do not significantly differ from those represented by J, except in that they (1) do not include regions of strong volume current such as that associated with the flux rope itself (compare, e.g., Figure 2 in this paper to Figure 5b in the work of *Fan and Gibson* [2006]), and (2) do not fall off as rapidly with height as isosurfaces of J do, which scale with the radially decreasing magnetic field strength. This sensitivity to magnetic field strength is a consequence of the finite grid spacing of the simulation: infinite resolution would, in principle, lead to sheets of infinite current density, independent of magnetic field strength (indeed, *Fan and Gibson* [2004] demonstrated that current density at the sheet increased with increasing grid resolution). Therefore the isosurfaces of J/B are a more insightful current-sheet representation, identifying regions of high diffusivity where reconnections are occurring.

[31] The red and orange field lines plotted in Figure 2c and Figure 4 intersect the orange isosurface shown in Figure 2e (the stronger of the two J/B values represented by the isosurfaces, shown in turquoise in Figure 4). Orange field lines are the subset that contain the dips removed from the filament plot of Figure 1e. As we will discuss in section 5 and show in Figure 5, the best way to trace reconnected field lines likely to be associated with coronal soft X-ray emission is to identify the field lines intersecting the current sheet at an initial time step, and then plot field lines at the next time step that originate from the initial set's footpoints but that diverge from these initial lines. For the quiescent case discussed in this section, as well as for the early stages of eruption discussed in section 5, the initial and subsequent sets of field lines do not greatly differ, because the reconnections that occur are essentially "interchange" reconnections between neighboring field lines. We will discuss this in more detail in section 5. For now we point out that that the red and orange field lines lie on both sides of the magenta, BPSS field lines. This is consistent with theory predicting reconnections between the sigmoidal, winding lines and the external, nonwinding lines when the BPSS is dynamically perturbed. The result of these reconnections is a gradual movement of the footpoints of the outermost, sigmoidal rope field lines toward the arcade photospheric boundary field (seen in Figure 2c as parallel blue and yellow stripes). This extension toward the arcade boundary by the sigmoidal field line footpoints can be seen clearly in Figures 2c and 4.

4.3. Soft X-Ray Sigmoid in Relation to the Quiescent Prominence

[32] Figure 4 shows the BPSS (magenta), stronger current sheet isosurface (shown in turquoise here), current sheet-intersecting fieldlines (red and orange), and filament dips (brown) all together, in order to facilitate study of the relationship between model-predicted filament and soft-X-ray sigmoid. As this image and those of Figure 2 show, the model proxies for filament (brown dips) and soft X-ray sigmoid (red and orange field-lines) are both centrally aligned above the photospheric neutral line, and show an inverse-S shape. The sigmoid has its footpoints anchored in the rope's photospheric magnetic bipole, while in contrast, the entire filament body is aligned with the neutral line. This is in agreement with the observed filament and soft X-ray sigmoid shown in Figure 2a–2b, and with observational studies of sigmoids and associated filaments [*Pevtsov*, 2002a, 2002b]. However, we disagree with the conclusion of those studies that the filament and soft X-ray sigmoid are separate magnetic structures. This conclusion was based largely on the fact that eruptive soft X-ray sigmoids have been observed in conjunction with nonerupting filaments lying apparently below them. As we will discuss in detail in section 5 and show in Figures 5 and 7c, an erupting sigmoid above a quiescent prominence may be explained by the breaking of a flux rope in two during eruption.

4.4. Cavity in Relation to the Quiescent Prominence

[33] Figure 3b demonstrates that the flux rope equilibrium intrinsically contains a cavity surrounding the prominence, in a manner that matches observations well. The model is isothermal, and so cannot treat the cooler prominence. However, it does explicitly treat gravity, and the density isosurface seen in a vertical slice through the rope in Figure 3b shows that there is a density enhancement along the axis of the rope where the dipped field lies. This central density enhancement is surrounded by a density depletion, i.e., a cavity, corresponding to sheared, nondipped field. This cavity arises from an expansion of the flux rope due to its strong axial magnetic field into the surrounding, initially potential field. The cavity has a more-or-less circular cross-section, arising from the circular cross section of the rope, and extends well above the top of the filament. Both of these properties are commonly observed in cavities, as is the sharp boundary of the cavity [*Gibson et al.*, 2006b]. In the case of our flux rope model the sharp boundary is explained by the magnetic flux surface between the rope and sur-

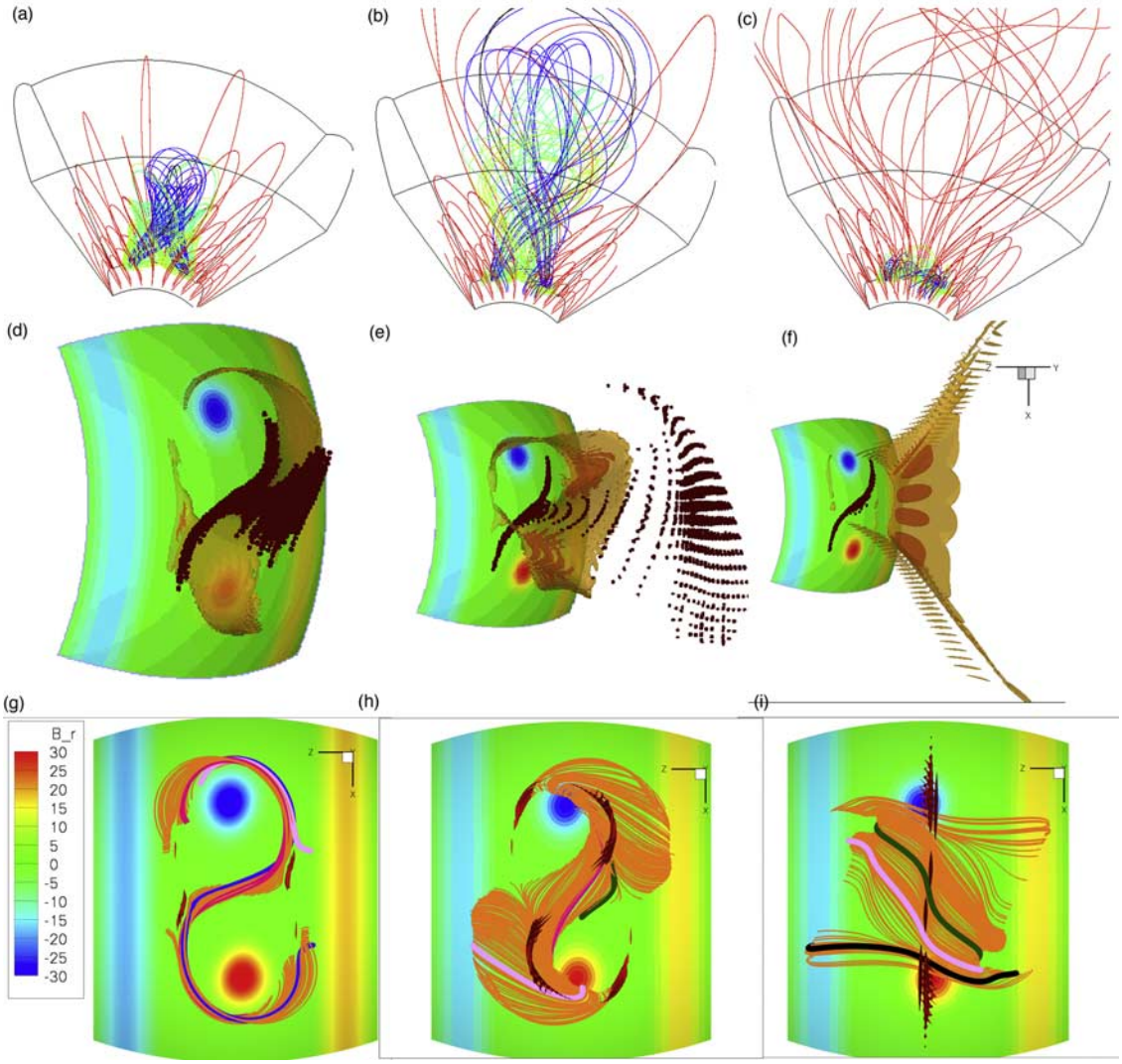

Figure 5. The eruption of a 3-D flux rope seen in snapshots at times (left column) t = 86 (when rope emergence is stopped) (middle column) t = 95 and (right column) t = 130 (top row) and t = 105 (middle and bottom rows) [*Gibson and Fan*, 2006]. (top) Sample field lines showing kinking, erupting rope: red lines are rooted in the original arcade boundary; blue and green field lines are rooted in the original rope bipole. (middle) Evolving, initially dipped field (brown) and current sheet isosurfaces (dark orange is approximately twice as strong a value of J/B as yellow). (bottom) Reconnected field lines (orange) associated with the stronger (dark orange) current sheet isosurface (shown here in red). The magenta, pink, dark green, blue, and black thicker lines are samples of different field line connectivities included in the reconnected field lines (see text and Table 1). The normal magnetic field is shown in Figures 5d–5i with contour levels identified in units of Gauss. Movies of the eruption corresponding to the three rows of this figure can be found in the electronic version of this paper.

rounding arcade across which mass and thermal energy cannot be transported in the highly conducting corona.

5. Energy Release Stage: Loss of Equilibrium

[34] We now turn to a different simulation, in which the rope was emerged to a degree where it lost equilibrium and erupted (Figure 5) [*Gibson and Fan*, 2006]. After an initial stage of quasi-static evolution where the total twist in the emerged tube was built up to about 1.7 winds between the anchored ends, the flux rope could no longer find a stable equilibrium and kinked and erupted through the arcade in a localized area with most of the arcade field remaining closed (see the top panels in Figure 5). The nonlinear evolution of the kink instability facilitated the eruption of the flux rope by changing its orientation at the apex, with the length-wise direction of the upward moving tube changing from being perpendicular to the arcade field to being parallel, so that the flux rope was able to push through the arcade field [*Fan*, 2005].

5.1. A Model for a Partial Prominence Eruption

[35] *Gibson and Fan* [2006] found that the flux rope did not erupt in entirety in this simulation, but that reconnec-

tions taking place in a central, vertical current sheet ultimately caused the flux rope to separate into two parts, with the upper part being ejected and the lower part left behind (see also *Birn et al.* [2006]). Figure 5 shows this eruption. Sample field lines rooted in the preeruption rope's normal magnetic field at the photosphere (the red and blue circular bipoles seen in the bottom images of Figure 5, referred to as the "rope bipole" from here on) are shown in blue and green in the top images. Sample field lines rooted in the preeruption surrounding arcade's normal magnetic field at the photosphere (the red and blue parallel stripes in the bottom images of Figure 5, referred to as the "arcade boundary" from here on) are shown in red in the top images. Figure 5c demonstrates that, due to a process of reconnections between the initial rope magnetic fields and the initial arcade magnetic fields (discussed in more detail below), the erupting rope ultimately is rooted in the arcade boundary, while the surviving rope is rooted in the rope bipole.

[36] Figures 5d–5f (and corresponding online movie) tracks the evolution of the the mass elements that sat on dipped field lines in the flux rope at the onset of the eruption (filled at that point, as in Figure 1c, up to a prominence scale height). We do this by using the local velocity vector at each point within the dips to determine (to second order) where material at that point would be transported to by the next time step, and so on through the eruption. As noted above, our simulations explicitly treat gravity and there is indeed a density enhancement in the dipped magnetic field that erupts outward as the core of the CME (Figures 8e–8h), but this material is necessarily at the (isothermal) coronal temperature of the simulation. To the extent magnetic energy density dominates the prominence gravitational energy density (i.e., to the extent the preeruption state is, as in our simulations, essentially "force-free"), the dynamic description of proxy filament material shown here should hold. It is important to acknowledge, however, that the coronal mass enhancement in the dipped magnetic field of our simulations is likely to underestimate the total mass contained in the erupting prominence [*Gilbert et al.*, 2005, 2006], and consequently we do not address the question of the potential role prominence mass may play in CME initiation and dynamics [*Low et al.*, 2003].

[37] Figures 5d–5f shows that our "filament" material generally evolved in one of three ways. If the mass sat on the lowest portion of the dipped field, below where the rope broke in two, it basically was unaffected by the eruption and maintained a sigmoid-shaped, surviving filament. If the mass lay near the central reconnections where the rope broke in two, it first accelerated upward, and then decelerated and fell back down to the surviving filament. Finally, if it lay on the higher portion of the dipped field, it was carried up and away by the erupting portion of the rope. We have discussed above how a range of factors would determine whether or not the dips were filled at the start of the eruption. The degree to which the initially dipped field was filled with filament mass, and the location of this mass relative to where the rope broke in two, would then determine whether all, some, or none of the filament would actually be observed to erupt and escape with the CME. That is, if all of the dips were filled, a partially erupting filament might be observed [*Tang*, 1986; *Gilbert et al.*, 2000; *Qiu and Yurchyshyn*, 2005], with some portion escaping, some surviving, and perhaps some first accelerating up and than falling back down [*Tripathi et al.*, 2006]. If only the upper dips were filled, the bulk of the filament might be ejected. If only the lower dips were filled, the filament might undergo a "failed eruption," with some temporary motion upward but no apparent ejection of material [*Ji et al.*, 2003], or it might not show any sign of eruption at all, despite activity occurring directly above it [*Pevtsov*, 2002a, 2002b; *Gibson et al.*, 2002].

5.2. Current Sheet Formation and Reconnecting Field Lines

[38] Figure 5 shows the evolution of the current sheets (as defined above) during the eruption. At the first time step (t = 86), there is a sigmoidal current sheet very similar to that of the equilibrium flux rope discussed in section 4 and shown in Figure 2e. As in that case, this current sheet lies essentially along the preeruption BPSS, with its strongest values of J/B at the "elbows" of the sigmoid, shown in Figures 5d–5f as dark orange isosurfaces. The current sheet also possesses a central portion that extends vertically and that is due to the squeezing together of the writhing rope legs. As the eruption progresses, that central, vertical component becomes the dominant current sheet of the system. It is important to note that this central, vertical current sheet does not extend all the way down to the photosphere. It is the location of the rope's breaking in two and ultimately where field lines close down behind the erupting portion of the rope.

[39] A variety of types of three-dimensional reconnections happen at these current sheets. Figure 6 demonstrates this. Early in the eruption, many of the reconnections are across the BPSS: essentially, a form of interchange reconnections between neighboring field lines. The blue field lines of Figure 6a exist at time t = 86, and are both part of the initial flux rope rooted in the rope bipole. However, the light blue field line is sigmoidal, and winds about the rope axis, while the dark blue field line lies outside the BPSS and, because it is essentially truncated by the photosphere, does not wind more than a full turn. These two field lines meet at the BPSS current sheet, in particular at the dark red isosurface shown in Figure 6a and its corresponding online movie. The reconnection of these field lines results in a swapping of footpoints, so that at time t = 87 a sigmoidal, winding magenta line emanates from the dark blue nonwinding line's footpoint, while a pink, nonwinding line extends from what was originally the footpoint of the pale blue sigmoidal line. We note that in this and the majority of reconnections we have followed, the system of field lines is not completely "closed." By this, we mean that two field lines at time t = 86 do not exactly map to two field lines at time t = 87. Close examination of Figure 6a and its corresponding online movie shows that the opposite footpoint of the magenta sigmoidal line is not exactly coincident with that of the pale blue sigmoid, and similarly the pale pink field line is not rooted in the dark blue line's footpoint. This indicates that further reconnections probably occurred, involving additional field lines not shown in Figure 6a. We will discuss this in more detail below in the context of Figure 6d.

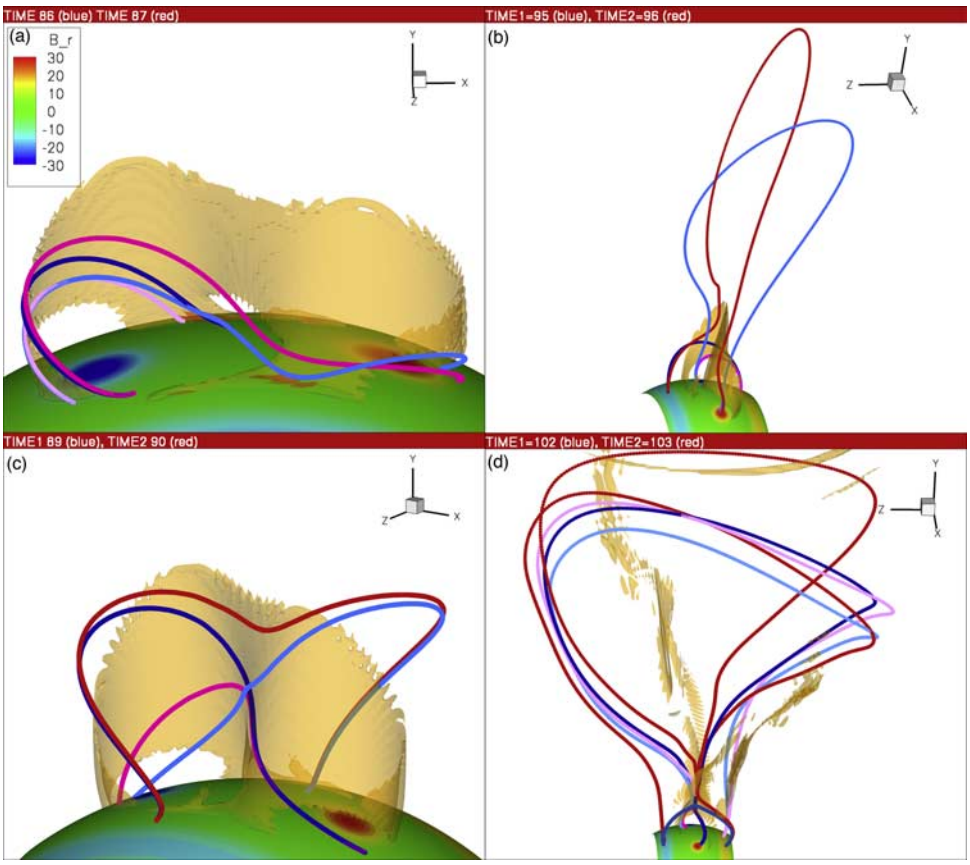

Figure 6. Four examples of common types of reconnection in the *Gibson and Fan* [2006] simulation: (a) interchange reconnection between neighboring field lines; (b) connectivity-mixing reconnection between rope and arcade; (c) reconnection at the central current sheet resulting in the breaking of the rope in two; and (d) multiple, simultaneous reconnections. The initial field lines are shown in shades of blue, and the final (subsequent time-step) field lines are shown in shades of red and pink. Current sheets are shown as semitransparent isosurface(s). The normal magnetic field is shown with contour levels identified in units of Gauss. Movies showing three-dimensional rotation of all four of these images can be found on the online version of this paper.

[40] Another thing to note about the pink field line in Figure 6a is that its outer footpoint extends toward the arcade boundary, in the manner discussed above with regards to the equilibrium rope simulation (this is especially clear in Figure 5g), which shows the pink and magenta field lines of Figure 6a from a top-down viewing angle). This implies that some of the further reconnections not explicitly shown in Figure 6a involved field lines rooted in the arcade boundary. Figure 6b demonstrates this second type of reconnection, which mixes the original two magnetic connectivities of rope and arcade. The lighter (and higher) of the two blue field lines at time $t = 95$ is completely rooted in the rope bipole, while the dark blue field is rooted in the arcade boundary. In what is, to the resolution of our field line plots, a closed system of reconnection, these two blue field lines map to the red and magenta field lines at time $t = 96$. The red field line is a winding, erupting flux rope with one leg in the rope bipole and the other in the arcade boundary, while the magenta line is a slightly sheared, nonerupting loop, also with one foot in each type of boundary.

[41] *Gibson and Fan* [2006] described how the bifurcation of the erupting flux rope occurred as a two-step process. The first step occurred as the rope writhed and rotated, bringing rope and arcade field lines in contact and facilitating connectivity-mixing reconnections such as shown in Figure 6b. The second step was a central reconnection, at the vertical current sheet between the rope legs, between mixed-connectivity field lines (e.g., the two blue field lines of Figure 6c). The results were erupting, arcade-boundary rooted field lines (e.g., the red field line of Figure 6c) and surviving, rope-bipole rooted field lines (e.g., the magenta field line of Figure 6c). In the case of Figure 6c, both the two initial, blue field lines, and the newly reconnected, red/magenta field lines are sigmoidal, winding lines. Not every central reconnection is of this type, Figure 4b in the work of *Gibson and Fan* [2006], for example, demonstrates a case where two mixed-connectivity, winding field lines reconnected to form an escaping, doubly twisted arcade-boundary-rooted line and a nonescaping, but nonwinding rope-bipole-rooted line. As discussed in that paper, and shown below in Figure 7c, the two ropes are separated by such nonwinding field lines. These lines transit smoothly from sheared lines which lie along the lower rope and are rooted in the rope bipole, to more potential field

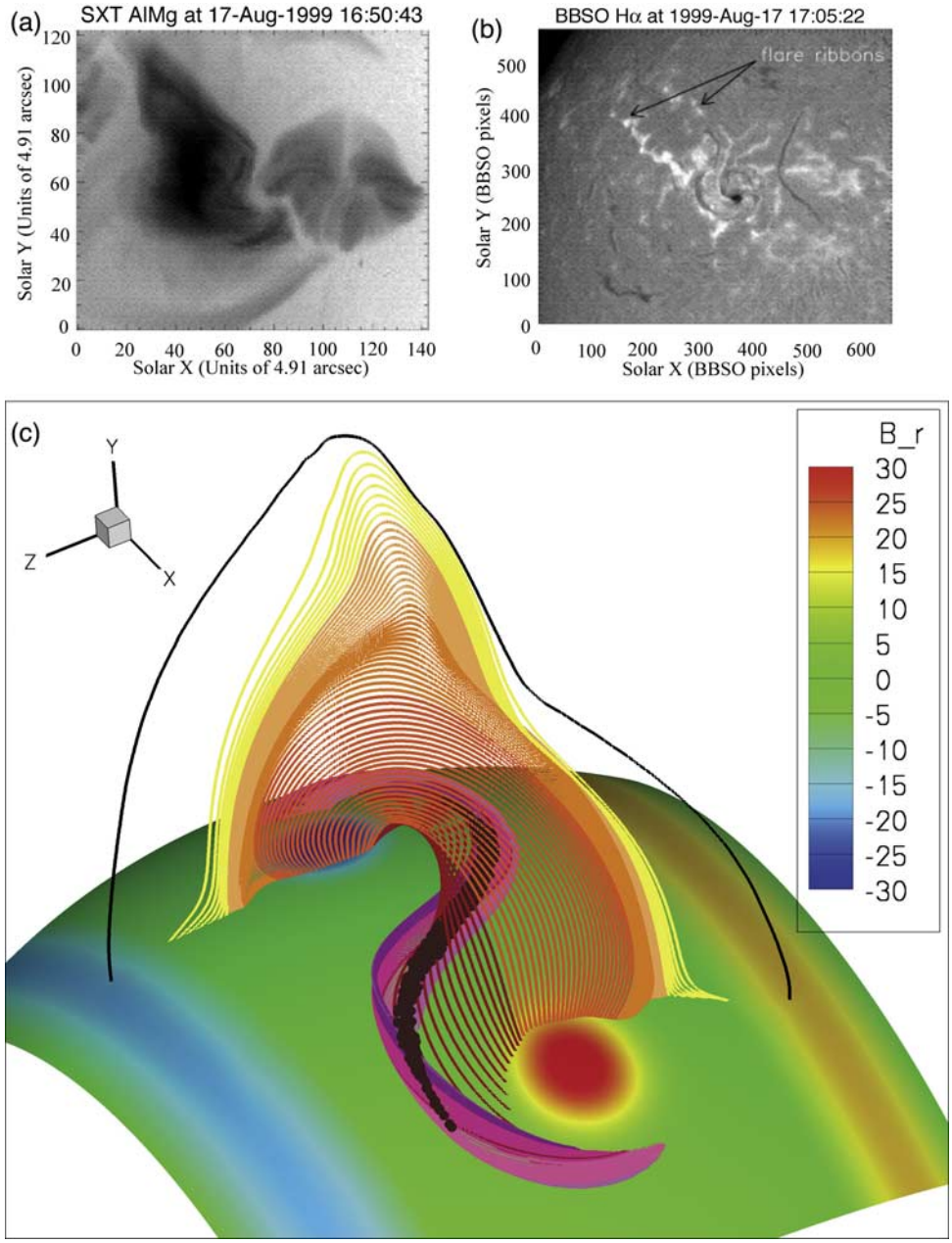

Figure 7. (a) Observation of a cusp forming over a sigmoid in soft-X-ray (Yohkoh SXT) and (b) associated, nonerupting H-α filament (BBSO) (from *Gibson et al.* [2002])(c) Posteruption state: cusp over sigmoid and filament. Magenta lines show BPSS of surviving rope, brown shows locus of the "filament" mass that survived eruption and lies within that rope, as followed in Figures 5d–5f. Red field lines above this are dipped (and so also possible location of filament formation). Orange field lines are rope-bipole-rooted loops, and black field line is a clearly arcade-boundary-rooted loop. The normal magnetic field is shown with contour levels identified in units of Gauss. A movie showing rotating in three dimensions as in Figure 7c can be found in the electronic version of this paper.

lines that straddle the lower rope and are rooted in the arcade boundary.

[42] Table 1 summarizes the field line connectivities present during the simulation, and references color-coded examples of each type in Figures 5 and 6. Three basic types are present prior to reconnections: winding field lines rooted in the rope-bipole (A), loops (with shear less than one full turn around rope axis) rooted in the rope-bipole (B), and loops rooted in the arcade-boundary (C). Interchange reconnections, such as shown in Figure 6a, may occur among field lines of types (A) and (B) and result in a swapping of field line footpoints, but no connectivity change. Rope-arcade reconnection, as shown in Figure 6b between field lines of type (A) and (C) (and/or between (B) and (C)) can create two new types of field lines, that is, winding field lines with one foot in the rope bipole and the other in the

Table 1. Summary of Connectivities

	Type	Color
	Present Prior to Reconnections	
A	Rope-bipole-rooted winding	magenta[a]
B	Rope-bipole-rooted loop	dark blue[b] and dark green[c]
C	Arcade-boundary-rooted loop	black[d]
	Present After Reconnections	
D	Mixed-connectivity-rooted winding	blue[e] and red[f]
E	Mixed-connectivity-rooted loop	pink[g]
F	Arcade-boundary-rooted winding	red[h]

[a]As shown in Figures 5g–5h; Figure 6a.
[b]As shown in Figure 6a.
[c]As shown in Figures 5h–5i.
[d]As shown in Figure 5i; Figure 7c.
[e]As shown in Figure 5g.
[f]As shown in Figure 6b.
[g]As shown in Figures 5g–5i; Figure 6a.
[h]As shown in Figure 6c–6d.

arcade boundary (D), and similarly mixed-connectivity loops (E). Two such mixed-connectivity winding field lines (D) are then able to reconnect at the central current sheet, breaking the rope into erupting, winding field lines rooted in the arcade-boundary (F), and surviving, rope-boundary rooted winding field lines and/or loops (restoring connectivities (A) and/or (B) to the system). Finally, some of the arcade-boundary rooted field may close down behind the erupting portion of the rope, thus restoring arcade-boundary rooted loops of type (C) at the interface between erupting and surviving ropes (e.g., the black field lines shown in Figures 5i and 7c.

[43] We conclude this section with a brief discussion on multiple reconnections. As noted above, most of the reconnecting field lines that we follow are not of the classic X-type, where two field lines reconnect and map to two new field lines. There are a few cases where such a simple reconnection appears to be happening, for example Figure 6b, and many more which are "almost" closed, in that the newly reconnected field line footpoints lie quite close to the initial pairs (e.g., Figures 6a and 6c). One possibility is simply that the two consecutive outputs from the simulation are too far apart in time to capture the reconnections occurring between them. Another is that, for a given instance, multiple reconnections are occurring along a single field line: this has been previously found to occur in the simulation of *Archontis et al.* [2005]. Figure 6d demonstrates how such multiple reconnections might occur in our simulations as well. In this case, the dark blue (tall) field line at time $t = 102$ reconnects with the light blue (tall) field line at the central current sheet, but simultaneously reconnects with the powder-blue (short) field line at the side current sheet between the rope and arcade. In the notation established above and in Table 1, field lines of connectivity types (A) (dark blue), (C) (powder blue), and (D) (pale blue) reconnect to form new field lines at time $t = 103$ of type (D) (pink), (F) red, and (B) (magenta). This demonstrates the complexity that may arise when reconnections occur in fully three dimensions.

5.3. Soft X-Ray Sigmoid in Relation to the Erupting Prominence

[44] Since magnetic energy is converted in part to thermal energy during reconnection and consequently heats the newly reconnected field lines, recently reconnected field lines may be identified with soft-X-ray sigmoids. We establish the evolution of such field lines in the following manner. First, we determine isosurfaces of J/B, as discussed above, to locate sharp gradients in the field where reconnections are likely to occur. We obtain the set of points that makes up the stronger, dark-orange isosurfaces shown in Figure 5d–5f, and trace the field lines intersecting these points (set 1). We then move one time step forward in our simulation, and trace field lines originating from the footpoints of set 1, creating a new set of field lines representing the field at the later time step (set 2). We then identify those field lines of set 2 which diverge from their corresponding set 1 field line by a distance greater than 0.1 $R_\odot$ (about 20 simulation grid steps). Finally, we plot only the subset of these diverging field lines whose apex is lower than 1.5 $R_\odot$, since soft X-ray emission falls off quickly with height.

[45] The result is the set of orange field lines shown in Figure 5g–5i. In the initial stages of the eruption, these map out a clear, backward-S sigmoid. As demonstrated by the highlighted colored field lines, connectivities of types (A), (D), and (E) are the products of these early, interchange and connectivity-changing type reconnections. As the eruption proceeds, connectivity-changing reconnections create many more of the pink, mixed-connectivity loops of type (E), which effectively broaden the sigmoid and extend it out to the arcade-boundary. As the central current sheet becomes dominant, rope-breaking reconnections restore rope-bipole rooted winding field lines of type (A), and, increasingly, less-sheared rope-bipole loops of type (B) that straddle the surviving rope. Finally, erupting arcade-boundary-rooted field lines close down, forming arcade-boundary loops of type (C). These, along with the type (B) and (E) loops appear to have a cusp shape when viewed along the surviving rope (Figure 7c). (Note that, because we limit ourselves to field lines lying below 1.5 $R_\odot$, erupting field lines of connectivities (D) and (F) are not represented in Figure 5g–5i.)

[46] We therefore see in our simulation a bright, transient eruptive sigmoid (Figure 5g) that transitions to a posteruption cusp forming below the expelled portion of the rope (Figure 7c), matching observations of soft X-ray sigmoid evolution [*Pevtsov*, 2002a, 2002b; *Gibson et al.*, 2002]. We note, however, that even after eruptions and sigmoid-to-cusp transitions, active regions can exhibit sigmoidal structures again within a matter of hours, or indeed simultaneously show a surviving sigmoid under a cusp (Figure 7a) [*Gibson et al.*, 2002]. In our simulation, we identify a BPSS associated with the nonerupting portion of the flux rope (magenta field lines in Figure 7c) which survives the eruption and lies below the cusped posteruption loops. Since the BPSS is likely to soon be dynamically perturbed, we would expect the persistent (e.g., noneruptive) soft X-ray sigmoid to quickly reform below the fading cusp, in the manner shown in Figure 7a.

[47] Comparing Figures 5d–5f and Figures 5g–5i, we now consider how the nonerupting portion of the filament compares to the evolving sigmoid. Initially, the relationship of this filament to the soft-X-ray sigmoid is much as described above for the quiescent case. As the current sheet extends higher, above the nonerupting filament (Figure 5e), the reconnected sigmoidal field lines likewise extend above

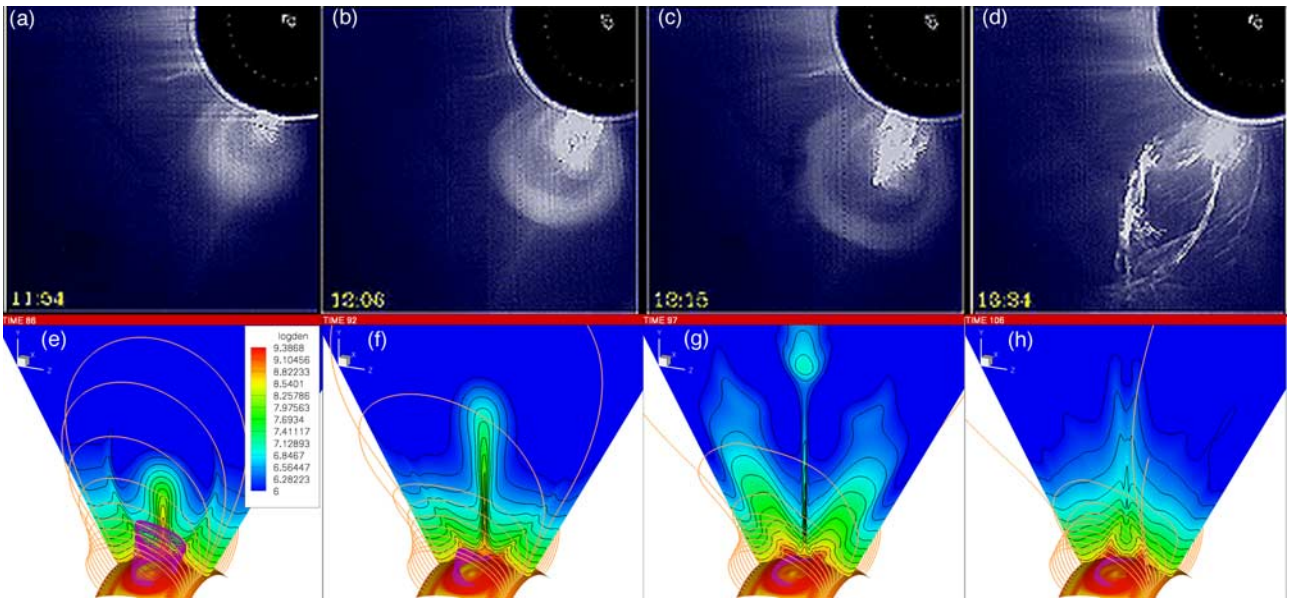

Figure 8. (top) Observation of three-part CME [*Illing and Hundhausen*, 1986] by the SMM coronagraph. (bottom) *Gibson and Fan* [2006] flux rope eruption. Isosurface and isocontours of the logarithm of density and field lines shown as in Figure 3. Isosurface and isocontours show the logarithm of number density (in cgs units). Movies of these observed and simulated eruptions can be found in the online version of this paper.

it. Finally, the cusped field lines form, also above the nonerupting filament. A sigmoid transitioning to a cusp above a nonerupting filament is often observed (e.g., Figures 7a–7b), and it has been argued that this implies that the sigmoid and filament are two separate magnetic structures *Pevtsov* [2002a, 2002b]. In our simulation, however, the eruptive sigmoid and noneruptive filament simply illustrate the two halves of the bifurcating flux rope. Finally, we note that the footpoints of the reconnected field lines shown in Figure 5i have begun to trace parallel lines along the arcade boundary, in a manner consistent with the two-ribbon flare seen on either side of the filament in Figure 7b.

5.4. Cavity in Relation to the Erupting Prominence

[48] Figures 8e–8h demonstrates that the result of the loss of equilibrium of the flux rope in our simulation is that the pre-CME structure of filament and surrounding cavity (e.g., Figure 3b) bodily lifts off as a three-part CME, possessing front, cavity, and core (e.g., Figures 8a–8d [*Illing and Hundhausen*, 1986]). Because the rope is only partially ejected, as the field lines close down over the surviving rope, a smaller cavity reforms around the non-ejected portion of the filament (Figure 8h and online movie). Both the bodily lifting off of cavities, and the immediate reforming of cavities posteruption, are observed [*Gibson et al.*, 2006b].

6. Discussion: Factors That Lead to Flux Rope Bifurcation During Eruption

[49] In the work of *Gibson and Fan* [2006] and *Gibson et al.* [2006a], we suggested that the combination of the modeled rope's three-dimensionality with the presence of a flux rope BP was responsible for its partial expulsion. We pointed out that three-dimensional flux rope models possessing an X-line-type topology below the rope, rather than a single, central, BP, have been demonstrated to erupt completely [*Toeroek and Kliem*, 2005]. Moreover, two-dimensional flux rope models possessing a central BP also can erupt totally, with a current sheet that extends below the erupting rope up from the photosphere [*Lin et al.*, 1998; *Fan and Gibson*, 2006]. The case discussed in this paper, on the other hand, shows that a three-dimensional flux rope with a single, central, BP may break in two during eruption. The combination of BPSS field lines which are not free to escape upward, with three-dimensional reconnections within the flux rope and between the flux rope and the ambient arcade field, results in the rope breaking in two.

[50] We extend this discussion now to consider the role of the kinking motion in facilitating the breaking of the rope. A twisted toroidal flux rope experiences an outward "hoop force" due to its toroidal current, while an external poloidal magnetic field (in which the toroidal flux rope is embedded) provides an inward confining force. If the external poloidal field decreases with distance sufficiently fast, a "torus instability" sets in where under a radially outward perturbation the hoop force dominates the confining force of the poloidal field and the toroidal flux rope can no longer be confined [*Bateman*, 1978; *Titov and Demoulin*, 1999; *Kliem and Toeroek*, 2006]. This has been demonstrated for a line-tied, three-dimensional flux rope without enough total twist to trigger the helical kink mode, but nevertheless which was found to erupt with little writhing as the torus instability set in the work of Kliem and Toeroek (presentation at the CCMAG meeting, Max Planck Institute for Solar System Research, Katlenburg-Lindau, Germany, 30 August to 2 September 2005). Y. Fan (manuscript in preparation, 2006) has undertaken an analysis of a three-dimensional flux rope possessing the same single, central, BP topology of *Gibson and Fan* [2006], but with an external poloidal

field that decreases with distance more rapidly and has also demonstrated such a torus-instability-triggered eruption with little writhing motion. In this case, like the axisymmetric case of *Fan and Gibson* [2006], a current sheet forms beneath the rope extending up from the photosphere and the flux rope is totally ejected. The implication is that, along with three-dimensionality and a single, central, BP, the writhing motion induced by the kink instability is essential in our simulations for forming a current sheet within the rope where it can break in two.

[51] It is interesting, in this context, to compare the splitting in two of our flux rope to that modeled in the simulation of *Manchester et al.* [2004]. In that simulation of the dynamic emergence of a magnetic flux rope across the photosphere, the rope ultimately reconnected internally along a current sheet and formed two ropes, one a relatively mass-free rope that escaped upward, and the other a low-lying, mass-loaded rope that remained behind. This simulation differed from ours in its explicit treatment of the dynamic emergence of the rope across the photosphere, and also in that it did not model a quiescent (sequence of quasi-static equilibria) stage because it did not include the restraining effect of an overlying arcade field. However, the manner in which their rope broke in two was essentially analogous to how ours did. Although there were no rotational motions induced by the kink instability as in our simulation, significant shearing motions induced by axial field gradients occurred oppositely directed across the neutral line, and were critical to the rope's bifurcation [*Manchester et al.*, 2004]. As in the simulation of *Gibson and Fan* [2006], these motions led to the formation of a current sheet within the rope, as opposed to a current sheet that extended beneath it down to the photosphere. The three-dimensional, rope-breaking reconnections then occurred along this internal current sheet.

[52] Whether or not a rope will bifurcate during eruption, then, most likely depends on whether current sheets form within or beneath the rope. Simulations show that the upward expansion of a rope leads to current sheet formation beneath it, in the vicinity of an X-line if one exists, but ultimately even for a rope with a BP, extending up from the photosphere. In order for the rope to break, an internal current sheet must form before this happens. In our simulation, the BP topology combines with the writhing of the rope to quickly form an internal current sheet, and so the rope breaks in two.

7. Conclusions

[53] In this paper, we have focussed on magnetic flux ropes. It is important to state that other magnetic structures are commonly used to model prominences, e.g., sheared magnetic arcades [*Antiochos et al.*, 1994]. Such models have been successful in matching a range of observations, including filament formation, structure, and dynamics [*Antiochos et al.*, 1999b, 2000; *Karpen et al.*, 2003, 2005, 2006], the triggering of CMEs and associated prominence eruptions [*Antiochos et al.*, 1999a], and partially erupting filaments [*Tokman and Bellan*, 2002]. Note, however, that hydrodynamic sheared-arcade analyses of filament formation and dynamics can be equally applied to a loosely wound flux rope, as we have done in section 4.1, because they are one-dimensional studies that do not distinguish between a dipped arcade field line and a flux rope field line that winds less than two full turns [*Antiochos et al.*, 2000]. Beyond this, the flux rope model provides a holistic explanation for observations of the prominence, cavity, and sigmoid, and their related evolution, to an extent that we assert is unmatched by sheared-arcade models.

[54] The results of this paper support our assertion: we have demonstrated that the partially ejected flux rope simulation of *Gibson and Fan* [2006] is physically consistent with a range of observations of prominences and associated coronal features. We find that the general structure and dynamics of quiescent prominences can be reproduced, along with their relationship to cavities and noneruptive soft X-ray sigmoids. Partially erupting filaments, sigmoids transitioning to cusps and back to sigmoids, and the bodily eruption of and reformation of coronal cavities can also be explained physically.

[55] We find, as *Archontis et al.* [2005] did, that the reconnections in our simulations probably occur at multiple points along a field line, and at angles that vary significantly from the two-dimensional X-point standard of 180 degrees (i.e., along rotational rather than tangential discontinuities). Although we must be cautious in our interpretation because of the limitations of numerical simulations, we expect that the Sun, being intrinsically three-dimensional, is likely to exhibit at least an equivalent degree of complexity. By explicitly tracking connectivity changes in our simulation, we gain insight into the possible nature of such three-dimensional reconnections in the corona.

[56] Finally, we find that the magnetic topology of a single, central BP in combination with writhing or shearing motions can lead to the formation of a current sheet within the rope. This internal current sheet, as opposed to a current sheet which extends down beneath it, allows the three-dimensional reconnections in the corona that break our flux rope in two.

[57] Our simulations to date have been idealized, rather than explicitly data-driven. Model parameters were chosen [see, e.g., *Fan*, 2005] to translate physically to a density, temperature, and magnetic field structure that would represent a plausible (if somewhat large) active region on the Sun. The rope's eruptive acceleration profile possesses the observed feature discussed by *Chen and Krall* [2003] of a well-defined period while it is still within 2 solar radii of the solar surface during which the acceleration peaks. (However, note that the peak acceleration occurs at a somewhat greater height, i.e., 1.35 solar radii from the solar surface, than that predicted by the scaling law of *Chen and Krall* [2003], i.e., 0.97 solar radii, which is 1.5 times the footpoint separation at the time of eruption. This may in part be because that scaling law does not take into account the additional acceleration associated with the writhing and rupture of the rope through the overlying arcade field [e.g., *Sturrock et al.*, 2001].) One could explicitly model a particular event of interest by choosing parameters to represent a flux rope with size and normal magnetic flux evolution that matches observations of emerging magnetic flux, and with the preexisting, overlying field likewise constrained by data (for example as a force-free extrapolation of observed preemergence fields). This is one likely route for future extensions of our analysis. However, we feel that it will

be important to complement such explicitly data-driven analyses with only slightly less idealized simulations than those presented here. Despite the simplicity of our initial model setup, its three-dimensionality in combination with the extensive interactions occurring between rope and pre-existing arcade led to a complex and dynamic system. It would be instructive to consider the effects of changing the preexisting overlying field to an asymmetric, but still potential, magnetic arcade, as a first step toward interpreting the quite probably far more complicated evolution of a rope emerging into magnetic fields prescribed by observations.

[58] The focus of this paper has been a comparison of the magnetic flux rope model to observations of prominences and related coronal structures. We conclude by reiterating that magnetic flux ropes are likely to be energetically favorable equilibrium states in the quiescent corona for regions that possess significant helicity. Moreover, analytical and numerical studies, including the one presented here, have demonstrated the loss of such flux rope equilibria can result in a CME-type eruption. Observationally and theoretically, the magnetic flux rope is a satisfying model for the prominence, in quiescence and in eruption.

[59] **Acknowledgments.** S. G. would like to thank Lisa, for sleeping quietly so that her mother could review this manuscript, and to congratulate Y. F. and Doug Braun on the birth of their daughter. We thank B. C. Low for internal HAO review of this paper, and Tom Holzer, Judy Karpen, Bernhard Kliem, Jim Klimchuk, Chip Manchester, and Tibor Toeroek for helpful discussions. S. G. thanks Spiro Antiochos and Mark Linton for organizing the DPP special session on magnetic flux tubes in space plasmas, and for the invitation to speak at this session. The Transition Region and Coronal Explorer, TRACE, is a mission of the Stanford Lockheed Institute for Space Research (a joint program of the Lockheed Martin Advanced Technology Center's Solar and Astrophysics Laboratory and Stanford's Solar Observatories Group), and part of the NASA Small Explorer program. The H-α images are courtesy of the Big Bear Solar Observatory/New Jersey Institute of Technology, and the He II image is courtesy of SOHO/EIT consortium. SOHO is a project of international cooperation between ESA and NASA. The Soft X-Ray Telescope (SXT) was prepared by the Lockheed Palo Alto Research Laboratory, the National Astronomical Observatory of Japan, and the University of Tokyo with the support of NASA and ISAS. Finally, the data from the Coronagraph/Polarimeter on board NASA's Solar Maximum Mission satellite and the Mark IV coronagraph at the Mauna Loa Solar Observatory are courtesy of the High Altitude Observatory, National Center for Atmospheric Research. The National Center for Atmospheric Research is sponsored by the National Science Foundation.

[60] Amitava Bhattacharjee thanks Terry Forbes and another reviewer for their assistance in evaluating this paper.

References

Abbett, W. P., and G. H. Fisher (2003), A coupled model for the emergence of active region magnetic flux into the solar corona, *Astrophys. J.*, *582*, 475.

Abbett, W. P., G. H. Fisher, and Y. Fan (2000), The three-dimensional evolution of rising, twisted magnetic flux tubes in a gravitationally stratified model, *Astrophys. J.*, *540*, 548.

Amari, T., J. F. Luciani, Z. Mikic, and J. Linker (1999), Three-dimensional solutions of magnetohydrodynamic equations for prominence magnetic support: Twisted magnetic flux rope, *Astrophys. J. Lett.*, *518*, 57.

Amari, T., J. F. Luciani, Z. Mikic, and J. Linker (2000), A twisted flux rope model for coronal mass ejections and two-ribbon flares, *Astrophys. J. Lett.*, *529*, 49.

Amari, T., J. F. Luciani, J. J. Aly, M. Z., and J. Linker (2003a), Coronal mass ejection: initiation, magnetic helicity, and flux ropes, ii. Turbulent diffusion-driven, *Astrophys. J.*, *595*, 1231.

Amari, T., J. F. Luciani, J. J. Aly, M. Z., and J. Linker (2003b), Coronal mass ejection: initiation, magnetic helicity, and flux ropes, i. Boundary motion-driven, *Astrophys. J.*, *585*, 1073.

Amari, T., J. F. Luciani, and J. J. Aly (2004a), Coronal magnetohydrodynamic evolution driven by subphotospheric conditions, *Astrophys. J. Lett.*, *615*, 165.

Amari, T., J. F. Luciani, and J. J. Aly (2004b), Non-current-free coronal closure of subphotospheric mhd models, *Astrophys. J. Lett.*, *629*, 37.

An, C.-H., S. T. Suess, and E. Tandberg-Hanssen (1985), On the formation of coronal cavities, *Sol. Phys.*, *102*, 165.

Antiochos, S. K., R. B. Dahlburg, and J. A. Klimchuk (1994), The magnetic field of solar prominences, *Astrophys. J. Lett.*, *420*, 41.

Antiochos, S. K., C. R. Devore, and J. A. Klimchuk (1999a), A model for solar coronal mass ejections, *Astrophys. J.*, *510*, 485.

Antiochos, S. K., P. J. MacNeice, D. S. Spicer, and J. A. Klimchuk (1999b), The dynamic formation of prominence condensations, *Astrophys. J.*, *512*, 985.

Antiochos, S. K., P. J. MacNeice, and D. S. Spicer (2000), The thermal nonequilibrium of prominences, *Astrophys. J.*, *536*, 494.

Archontis, V., F. Moreno-Insertis, K. Galsgaard, A. Hood, and E. O'Shea (2004), Emergence of magnetic flux from the convection zone into the corona, *Astron. Astrophys.*, *426*, 1047.

Archontis, V., F. Moreno-Insertis, K. Galsgaard, and A. W. Hood (2005), The three-dimensional interaction between emerging magnetic flux and a large-scale coronal field: Reconnection, current sheets, and jets, *Astrophys. J.*, *635*, 1299.

Athay, R. G., and T. E. Holzer (1982), The role of spicules in heating the solar atmosphere, *Astrophys. J.*, *255*, 743.

Aulanier, G., and P. Demoulin (1998), 3-d magnetic configurations supporting prominences, I. The natural presence of lateral feet, *Astron. Astrophys.*, *329*, 1125.

Aulanier, G., P. Demoulin, and R. Grappin (2005), Equilibrium and observational properties of line-tied twisted flux tubes, *Astron. Astrophys.*, *430*, 1067.

Bateman, G. (1978), *MHD Instabilities*, pp. 84–85, MIT Press, Cambridge, Mass.

Berger, M. A., and G. B. Field (1984), The topological properties of magnetic helicity, *J. Fluid Mech.*, *147*, 133.

Birn, J. T., T. G. Hesse, and M. Hesse (2006), Stability and dynamic evolution of three-dimensional flux ropes, *J. Geophys.*, *845*, 732.

Canfield, R. C., H. S. Hudson, and D. E. McKenzie (1999), Sigmoidal morphology and eruptive solar activity, *Geophys. Res. Lett.*, *26*, 627.

Chen, J., and J. Krall (2003), Acceleration of coronal mass ejections, *J. Geophys. Res.*, *108*(AX), 1410, doi:10.1029/2003JA009849.

Cremades, H., and V. Bothmer (2004), On the three-dimensional configuration of coronal mass ejections, *Astron. Astrophys.*, *422*, 307.

Dere, K. P., G. E. Brueckner, R. A. Howard, D. J. Michels, and J. P. Delaboudiniere (1998), Lasco and eit observations of helical structure in coronal mass ejections, *Astrophys. J.*, *492*, 804.

Emonet, T., and F. Moreno-Insertis (1998), The physics of twisted magnetic tubes rising in a stratified medium: Two-dimensional results, *Astrophys. J.*, *492*, 804.

Fan, Y. (2001), The emergence of a twisted Ω-tube into the solar atmosphere, *Astrophys. J. Lett.*, *554*, 111.

Fan, Y. (2005), Coronal mass ejections as loss of confinement of kinked magnetic flux ropes, *Astrophys. J.*, *630*, 543.

Fan, Y., and S. E. Gibson (2004), Numerical simulations of three-dimensional coronal magnetic fields resulting from the emergence of twisted magnetic flux tubes, *Astrophys. J.*, *609*, 1123.

Fan, Y., and S. E. Gibson (2006), On the nature of the x-ray bright core in a stable filament channel, *Astrophys. J. Lett.*

Fan, Y., E. G. Zweibel, M. G. Linton, and G. H. Fisher (1998), The rise of kink-unstable magnetic flux tubes in the solar convection zone, *Astrophys. J. Lett.*, *505*, 59.

Forbes, T. G., and E. R. Priest (1995), Photospheric magnetic field evolution and eruptive flares, *Astrophys. J.*, *446*, 377.

Galsgaard, K., and A. W. Longbottom (1999), Formation of solar prominences by flux convergence, *Astrophys. J.*, *510*, 444.

Gibson, S. E., and Y. Fan (2006), The partial expulsion of a magnetic flux rope, *Astrophys. J. Lett.*, *637*, 65.

Gibson, S. E., and B. C. Low (1998), A time-dependent three-dimensional magnetohydrodynamic model of the coronal mass ejection, *Astrophys. J.*, *493*, 460.

Gibson, S. E., and B. C. Low (2000), Three-dimensional and twisted: An mhd interpretation of on-disk observational characteristics of coronal mass ejections, *J. Geophys. Res.*, *105*, 18,187.

Gibson, S. E., et al. (2002), The structure and evolution of a sigmoidal active region, *Astrophys. J.*, *574*, 265.

Gibson, S. E., B. C. Low, K. D. Leka, Y. Fan, and L. Fletcher (2003), Magnetic flux ropes: Would we know one if we saw one?, in *Magnetic Coupling in the Solar Atmosphere: Proceedings of IAU*, *Eur. Space Agency Spec. Publ., ESA-SP 505*, 65.

Gibson, S. E., Y. Fan, C. Mandrini, G. Fisher, and P. Demoulin (2004), Observational consequences of a magnetic flux rope emerging into the corona, *Astrophys. Journ.*, *617*, 600.

Gibson, S. E., Y. Fan, T. Toeroek, and B. Kliem (2006a), The evolving sigmoid: Evidence for magnetic flux ropes in the corona before, during,

and after cmes, in *Solar Dynamics and its Effects on the Heliosphere and Earth*, Springer, New York.
Gibson, S. E., D. Foster, J. Burkepile, G. de Toma, and S. A. (2006b), The calm before the storm: The link between quiescent cavities and cmes, *Astrophys. J.*, *641*, 590.
Gilbert, H. R., T. E. Holzer, J. T. Burkepile, and A. J. Hundhausen (2000), Active and eruptive prominences and their relationship to coronal mass ejections, *Astrophys. J.*, *537*, 503.
Gilbert, H. R., T. E. Holzer, and J. T. Burkepile (2001), Observational interpretation of an active prominence on 1999 May 1, *Astrophys. J.*, *549*, 1221.
Gilbert, H. R., T. E. Holzer, and R. M. MacQueen (2005), A new technique for deriving prominence mass from soho eit fe xii (19.5 nm) absorption features, *Astrophys. J.*, *618*, 524.
Gilbert, H. R., L. E. Falco, T. E. Holzer, and R. M. MacQueen (2006), Application of a new technique for deriving prominence mass from soho eit fe xii (19.5 nm) absorption features, *Astrophys. J.*, *641*, 606.
Gosling, J. T., E. Hildner, R. M. MacQueen, R. H. Munro, A. I. Poland, and C. L. Ross (1974), Mass ejections from the Sun: A view from skylab, *J. Geophys. Res.*, *79*, 4581.
Gosling, J. T., J. Birn, and M. Hesse (1995), Three-dimensional magnetic reconnection and the magnetic topology of coronal mass ejection events, *Geophys. Res. Lett.*, *22*, 869.
Hudson, H. S., L. W. Acton, K. A. Harvey, and D. M. McKenzie (1999), A stable filament cavity with a hot core, *Astrophys. J.*, *513*, 83.
Illing, R. M., and A. J. Hundhausen (1986), Disruption of a coronal streamer by an eruptive prominence and coronal mass ejection, *J. Geophys. Res.*, *91*, 10,951.
Ji, H., H. Wang, E. J. Schmahl, Y.-J. Moon, and Y. Jiang (2003), Observations of the failed eruption of a filament, *Astrophys. J.*, *595*, 135.
Karpen, J. T., S. K. Antiochos, M. Hohensee, and J. A. Klimchuk (2001), Are magnetic dips necessary for prominence formation, *Astrophys. J.*, *553*, 85.
Karpen, J. T., S. K. Antiochos, J. A. Klimchuk, and P. J. MacNeice (2003), Constraints on the magnetic field geometry in prominences, *Astrophys. J.*, *593*, 1187.
Karpen, J. T., S. E. M. Tanner, S. K. Antiochos, and C. R. DeVore (2005), Prominence formation by thermal nonequilibrium in the sheared-arcade model, *Astrophys. J.*, *635*, 1319.
Karpen, J. T., S. K. Antiochos, and J. A. Klimchuk (2006), The origin of high-speed motions and threads in prominences, *Astrophys. J.*, *637*, 531.
Kliem, B., and T. Toeroek (2006), Torus instability, *Phys. Rev. Lett.*, *96*, 255,002.
Kliem, B., V. S. Titov, and T. Toeroek (2004), Formation of current sheets and sigmoidal structure by the kink instability of a magnetic loop, *Astron. Astrophys.*, *413*, 23.
Kuperus, M., and M. A. Raadu (1974), The support of prominences formed in neutral sheets, *Astron. Astrophys.*, *31*, 189.
Kusano, K. (2005), Simulation study of the formation mechanism of sigmoidal structure in the solar corona, *Astrophys. J.*, *631*, 1260.
Kusano, K., T. Maeshiro, T. Yokoyama, and T. Sakurai (2004), The trigger mechanism of solar flares in a coronal arcade with reversed magnetic shear, *Astrophys. Journ.*, *610*, 549.
Leka, K. D., R. C. Canfield, A. N. McClymont, and L. van Driel-Gesztelyi (1996), Evidence for current-carrying emerging flux, *Astrophys. J.*, *462*, 547.
Leroy, J. L., V. Bommier, and S. Sahal-Brechot (1984), New data on the magnetic structure of quiescent prominences, *Astron. Astrophys.*, *131*, 33.
Lin, J., T. G. Forbes, P. A. Isenberg, and P. Demoulin (1998), The effect of curvature on flux rope models of coronal mass ejections, *Astrophys. J.*, *504*, 1006.
Lindsay, G. M., J. G. Luhmann, C. T. Russell, and J. T. Gosling (1999), Relationships between coronal mass ejection speeds from coronagraph images and interplanetary characteristics of associated interplanetary coronal mass ejections, *J. Geophys. Res.*, *104*, 12,515.
Linker, J., R. Lionello, Z. Mikic, and T. Amari (2001), Magnetohydrodynamic modeling of prominence formation within a helmet streamer, *J. Geophys. Res.*, *106*, 25,165.
Linker, J., Z. Mikic, R. Lionello, P. Riley, T. Amari, and D. Odtrcil (2003), Paper title?, *Phys. Plasmas*, *10*, 1971.
Lionello, R., Z. Mikic, and J. A. Linker (2002), Magnetic field topology in prominences, *Astrophys. J.*, *581*, 718.
Lites, B. W., and B. C. Low (1997), Flux emergence and prominences: a new scenario for 3-dimensional field geometry based on observations with the advanced stokes polarimeter, *Sol. Phys.*, *174*, 91.
Litvinenko, Y. E., and M. S. Wheatland (2005), A simple dynamical model for filament formation in the solar corona, *Astrophys. J.*, *630*, 587.
Longcope, D. W., and B. T. Welsch (2000), A model for the emergence of a twisted magnetic flux tube, *Astrophys. J.*, *545*, 1089.
Low, B. C. (1996), Solar activity and the corona, *Sol. Phys.*, *167*, 217.
Low, B. C. (2001), Coronal mass ejections, magnetic flux ropes, and solar magnetism, *J. Geophys. Res.*, *106*, 25,141.
Low, B. C., and M. Berger (2003), A morphological study of helical coronal magnetic structures, *Astrophys. J.*, *589*, 644.
Low, B. C., and J. R. Hundhausen (1995), Magnetostatic structures of the solar corona. ii. the magnetic topology of quiescent prominences, *Astrophys. J.*, *443*, 818.
Low, B. C., and G. J. D. Petrie (2005), The internal structures and dynamics of solar quiescent prominences, *Astrophys. J.*, *626*, 551.
Low, B. C., B. Fong, and Y. Fan (2003), The mass of a solar quiescent prominence, *Astrophys. J.*, *594*, 1060.
Lynch, B. J., S. K. Antiochos, P. J. MacNeice, F. T. H. Zurbuchen, and L. A. (2004), Observable properties of the breakout model for coronal mass ejections, *Astrophys. J.*, *617*, 589.
Mackay, D. H., and A. A. van Ballegooijen (2001), A possible solar cycle dependence to the hemispheric pattern of filament magnetic fields?, *Astrophys. J.*, *560*, 445.
Mackay, D. H., and A. A. van Ballegooijen (2005), New results in modeling the hemispheric pattern of solar filaments, *Astrophys. J. Lett.*, *621*, 77.
Mackay, D. H., and A. A. van Ballegooijen (2006), Models of the large-scale corona. Formation, I., evolution, and liftoff of magnetic flux ropes, *Astrophys. J.*, *641*, 577.
Magara, T. (2004), A model for dynamic evolution of emerging magnetic fields in the sun, *Astrophys. J.*, *605*, 480.
Magara, T., and D. Longcope (2001), Sigmoid structure of an emerging flux tube, *Astrophys. J. Lett.*, *559*, 55.
Manchester, W., T. Gombosi, D. DeZeeuw, and Y. Fan (2004), Eruption of a buoyantly emerging magnetic flux rope, *Astrophys. J.*, *610*, 588.
Manoharan, P. K., L. van Driel-Gesztelyi, M. Pick, and P. Demoulin (1996), Evidence for large-scale solar magnetic reconnection from radio and x-ray measurements, *Astrophys. J. Lett.*, *468*, 73.
Martin, S. F. (1998), Conditions for the formaiton and maintenance of filaments, *Sol. Phys.*, *182*, 107.
Parker, E. N. (1994), *Spontaneous Current Sheets in Magnetic Fields With Applications to Stellar X Rays*, Oxford Univ. Press, New York.
Petrie, G. J. D., and B. C. Low (2005), The dynamical consequences of spontaneous current sheets in quiescent prominences, *Astrophys. J. Supp.*, *159*, 288.
Pevtsov, A. A. (2002a), Active-region filaments and x-ray sigmoids, *Sol. Phys.*, *207*, 111.
Pevtsov, A. A. (2002b), Sinuous coronal loops at the sun, in *Yohkoh 10th Anniversary Meeting Proceedings*, *COSPAR Colloq. Ser.*, edited by P. C. H. Martens and D. Cauffman, p. 125, Elsevier, New York.
Plunkett, S. P., A. Vourlidas, S. Simberova, M. Karlicky, P. Kotric, P. Heinzel, Y. A. Kupryakov, W. P. Guo, and S. T. Wu (2000), Simultaneous soho and ground-based observations of a large eruptive prominence and coronal mass ejection, *Sol. Phys.*, *194*, 371.
Pneuman, G. W. (1983), The formation of solar prominences by magnetic reconnection and condensation, *Sol. Phys.*, *88*, 219.
Priest, E. R., and T. G. Forbes (2002), The magnetic nature of solar flares, *Astron. Astrophys. Rev.*, *10*, 313.
Priest, E. R., A. W. Hood, and U. Anzer (1989), A twisted flux-tube model for solar prominences. I- General properties, *Astrophys. J.*, *344*, 1010.
Qiu, J., and V. B. Yurchyshyn (2005), Magnetic reconnection flux and coronal mass ejection velocity, *Astrophys. J. Lett.*, *634*, 121.
Roussev, I. L., I. V. Sokolov, T. G. Forbes, T. I. Gombosi, M. A. Lee, and J. I. Sakai (2004), A numerical model of a coronal mass ejection: Shock development with implications for the acceleration of gev protons, *Astrophys. J.*, *605*, 73.
Rust, D. M., and A. Kumar (1994), Helical magnetic field in filaments, *Sol. Phys.*, *155*, 69.
Rust, D. M., and A. Kumar (1996), Evidence for helically kinked magnetic flux ropes in solar eruptions, *Astrophys. J.*, *464*, 199.
Saito, K., and E. Tandberg-Hanssen (1973), The arch systems, cavities, and prominences in the helmet streamer observed at the solar eclipse, november 12, 1966, *Sol. Phys.*, *31*, 105.
Sterling, A. C., and H. S. Hudson (1997), Yohkoh sxt observations of x-ray dimming associated with a halo coronal mass ejection, *Astrophys. J.*, *491*, 55.
Stone, J. M., and M. L. Norman (1992), Zeus-2d: A radiation magnetohydrodynamics code for astrophysical flows in two space dimensions. I- The hydrodynamic algorithms and tests, *Astrophys. J. Suppl.*, *80*, 753.
Sturrock, P. A., M. Weber, M. S. Wheatland, and R. Wolfson (2001), Metastable magnetic configurations and their significance for solar eruptive events, *Astrophys. J.*, *548*, 492.
Tanaka, K. (1991), Studies on a very flare-active delta group - peculiar delta spot evolution and inferred subsurface magnetic rope structure, *Sol. Phys.*, *36*, 133.

Tang, F. (1986), Studies on a very flare-active delta group - peculiar delta spot evolution and inferred subsurface magnetic rope structure, *Sol. Phys.*, *105*, 399.

Titov, V. S., and P. Demoulin (1999), Basic topology of twisted magnetic configurations in solar flares, *Astron. Astrophys.*, *351*, 707.

Titov, V. S., E. R. Priest, and P. Demoulin (1993), Conditions for appearances of "bald patches" at the solar surface, *Astron. Astrophys.*, *276*, 564.

Toeroek, T., and B. Kliem (2003), The evolution of twisting coronal magnetic flux tubes, *Astron. Astrophys.*, *406*, 1043.

Toeroek, T., and B. Kliem (2005), Confined and ejective eruptions of kink-unstable flux ropes, *Astrophys. J. Lett.*, *630*, 97.

Tokman, M., and P. M. Bellan (2002), Three-dimensional model of the structure and evolution of coronal mass ejections, *Astrophys. J.*, *567*, 1202.

Tripathi, D., S. K. Solanki, R. Schwenn, V. Bothmer, M. Mierla, and G. Stenborg (2006), Observation of a bright coronal downflow by SOHO/EIT, *Astron. Astrophys.*, *449*, 369.

van Ballegooijen, A. A. (2004), Observations and modeling of a filament on the sun, *Astrophys. J.*, *612*, 519.

van Ballegooijen, A. A., and P. C. H. Martens (1999), Formation and eruption of solar prominences, *Astrophys. J.*, *343*, 971.

van Ballegooijen, A. A., N. P. Cartledge, and E. R. Priest 1998, Magnetic flux transport and the formation of filament channels on the sun, *Astrophys. J.*, *501*, 866.

van Ballegooijen, A. A., E. R. Priest, and D. H. Mackay (2000), Mean field model for the formation of filament channels on the sun, *Astrophys. J.*, *539*, 983.

Webb, D. F., E. W. Cliver, N. U. Crooker, O. C. St. Cyr, and B. J. Thompson (2000), Relationship of halo coronal mass ejections, magnetic clouds, and magnetic storms, *J. Geophys. Res.*, *105*, 7491.

Zhang, M., and B. C. Low (2005), The hydromagnetic nature of solar coronal mass ejections, *Annu. Rev. Astron. Astrophys.*, *43*, 103.

Zirker, J. B., O. Engvold, and S. F. Martin (1998), Counter-streaming gas flows in solar prominences as evidence for vertical magnetic fields, *Science*, *396*, 440.

Y. Fan and S. E. Gibson, High Altitude Observatory, National Center for Atmospheric Research, P. O. Box 3000, Boulder, CO 80307-3000, USA. (sgibson@hao.ucar.edu)